https://doi.org/10.5194/egusphere-2025-3462
Preprint. Discussion started: 17 November 2025

Climate Impacts on Water Resources in a High Mountain Catchment: Application of the Open-Source Modeling Workflow MATILDA in the Northern Tian Shan

Phillip Schuster[1,*], Azamat Osmonov[2], Alexander Georgi[1], Christoph Schneider[1], and Tobias Sauter[1]

[1]Geography Department, Humboldt-Universität zu Berlin, Unter den Linden 6, 10099 Berlin, Germany
[2]Department of Climate, Water and Natural Resources, Central Asian Institute for Applied Geosciences, Timur Frunze Rd.73/2, 720027 Bishkek, Kyrgyzstan
[*]Corresponding Author

Correspondence: Phillip Schuster (phillip.schuster@geo.hu-berlin.de)

Abstract. Applied glacio-hydrological modeling is crucial for the integrated water management strategies needed to effectively mitigate climate change impacts on freshwater resources fed by high mountain areas. We demonstrate the application of MATILDA-Online, an open-source toolkit for modeling glacier evolution and water resources in glacierized catchments. We showcase it's capabilities in data-scarce environments on a catchment in the Tian Shan Mountains in Kyrgyzstan, and outline a four-step multi-objective calibration strategy that integrates glacier surface mass balance, snow water equivalent, and discharge observations. Projections indicate severe glacier mass loss by 2100, significant reductions in runoff, and a shift toward earlier peak flow driven by snowmelt. The main sources of uncertainty in the catchment water balance are biases in precipitation data and inconsistencies in glacier mass balance datasets, highlighting the importance of adequate monitoring. Despite limitations in the model's representation of spatial variability and dynamic processes, MATILDA provides easy access to sophisticated modeling and can be a valuable tool for bridging the gap between advanced glacio-hydrological science and practical water resource management.

1 Introduction

The freshwater resources of almost a quarter of the world's population are highly vulnerable to changes in the cryosphere of high mountain headwaters (Hock et al., 2019; Viviroli et al., 2020; Immerzeel et al., 2020; Aggarwal et al., 2022). Glacio-hydrological modeling is essential for implementing the integrated water management strategies needed to effectively mitigate climate change impacts in these regions (Hock et al., 2019; van Tiel et al., 2020). In part 1 of this double publication (Schuster et al., 2025c) we present the open source toolkit for **M**odeling glacier evolution and w**AT**er resources **I**n meso-scale g**L**acierize**D** c**A**tchments (MATILDA). It facilitates access to advanced modeling routines, datasets, and tools for professionals in the Global South, students, and researchers. In the present study, we apply the toolkit to assess climate impacts on the freshwater resources in a glacierized catchment in Kyrgyzstan.

Central Asia is one of the most vulnerable regions to water-related impacts of climate change. The majority of the region's population depends on water supplies from the Tian Shan Mountains (Hagg et al., 2007; Sorg et al., 2012). In the semi-arid to

https://doi.org/10.5194/egusphere-2025-3462
Preprint. Discussion started: 17 November 2025

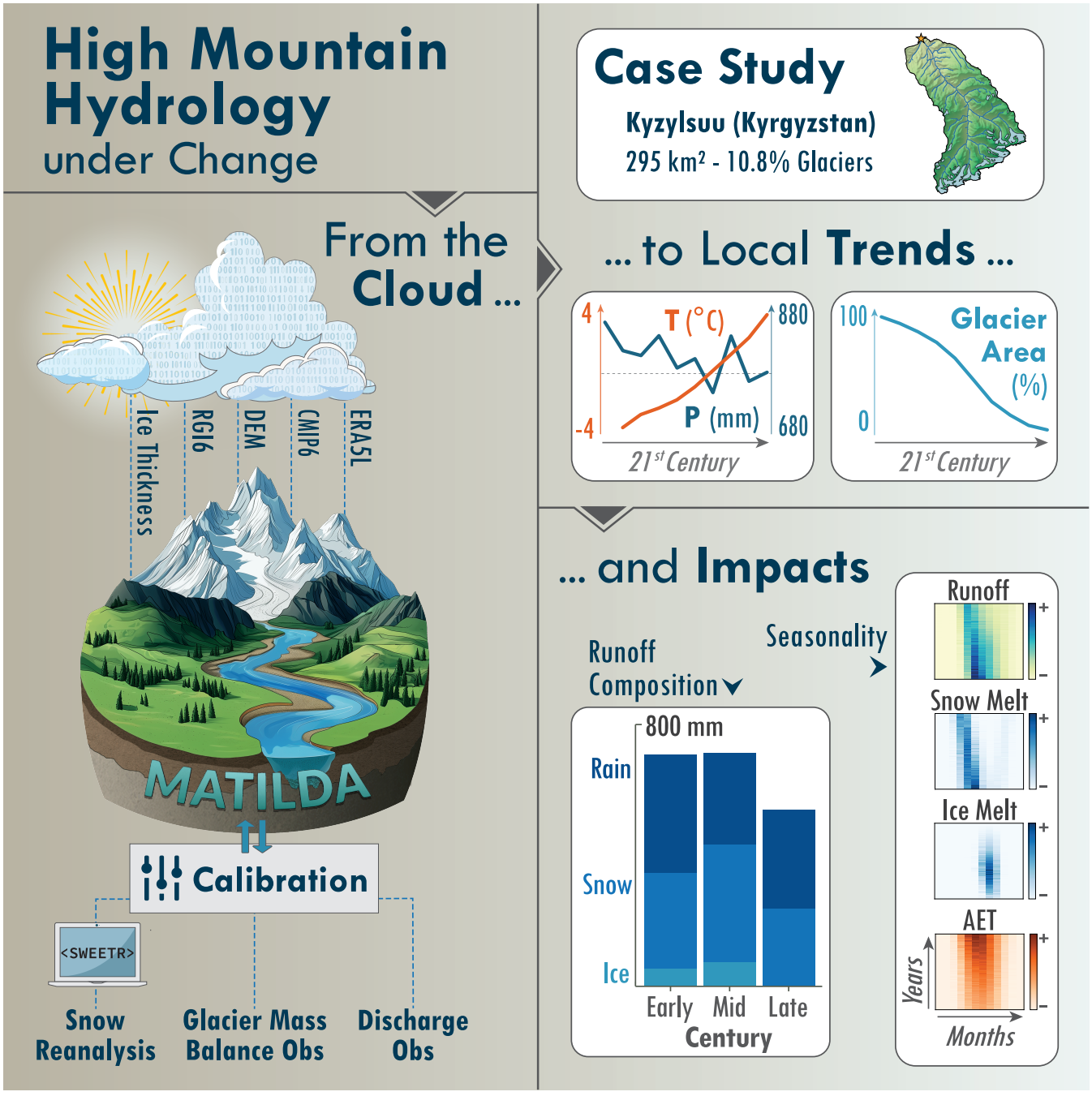

Graphical Abstract

https://doi.org/10.5194/egusphere-2025-3462
Preprint. Discussion started: 17 November 2025

arid continental climate, glacier melt can account for 15 to 69 % of the annual runoff in the region's river systems (Aizen et al., 1995, 1996; Dickich and Hagg, 2004; Hagg et al., 2007). Central Asia is also particularly vulnerable to water-related political tensions (De Stefano et al., 2017; Hock et al., 2019). The complex political geography of the region, coupled with the uneven distribution of renewable water resources, water consumption, and economic development (Chen et al., 2018; Zhang et al., 2020), leads to recurrent international disputes over water allocation (Bernauer and Siegfried, 2012; Peña-Ramos et al., 2021). These issues may be exacerbated by changes in the hydrological regimes associated with climate change (Bocchiola et al., 2017; Chen et al., 2018; Hock et al., 2019). As a consequence of rising temperatures (Aizen et al., 1997), less precipitation falls as snow (Chen et al., 2016; Yang et al., 2019; Li et al., 2020) and glacial melt rates increase (Bolch, 2007; Bolch et al., 2009). Consequently, Central Asia has lost over 25 % of its total glacier mass since 1961 (Farinotti et al., 2015). Some studies predict that another $\tilde{5}0$ % of today's glacier area (Lutz et al., 2014) or mass (Farinotti et al., 2015) will disappear by 2050. Others predict a less rapid, but still concerning, decline of at least 30 % in ice volume by 2100 (Miles et al., 2021).

The ongoing cryospheric changes are profoundly altering the regional hydrology by shifting the timing of peak flows to earlier in the year and reducing summer runoff (Sorg et al., 2012; Kriegel et al., 2013; Chen et al., 2018; Barandun et al., 2020; Shannon et al., 2023; Siegfried et al., 2024). Increasing evaporative losses associated with rising temperatures aggravated agricultural droughts throughout the region (Gerlitz et al., 2020; Jiang and Zhou, 2023). Since glaciers play a crucial role in mitigating drought stress (Pohl et al., 2017; Pritchard, 2019; Van Tiel et al., 2021), drought frequency and intensity are expected to further increase in the future (Hua et al., 2022; Wu et al., 2025). While the general trends are well understood at the global and regional scale, the hydrological response to climate change varies significantly across Central Asia (Siegfried et al., 2024) and its implications for water availability and extremes at the local scale remain poorly constrained (Barandun et al., 2020; Siegfried et al., 2024). Since these impacts are most relevant to local stakeholders, facilitating access to modern modeling tools and datasets for impact assessments at finer spatial scales is key to reducing the local population's vulnerability to water stress (Gerlitz et al., 2020; Barandun et al., 2020).

MATILDA-Online (Schuster et al., 2025a) is designed to meet the needs of an accessible modeling tool in contexts of limited observations. In this study, we use it to investigate the impact of 21st-century climate change on the water balance of a glacierized catchment in the Kyrgyz Tian Shan (see figure 1) and to evaluate the proposed data products in the light of scarce observations. We also present a multi-objective calibration approach, assess model uncertainty, and discuss limitations. This study lays the groundwork for improving localized climate impact assessment in glacierized catchments with limited monitoring. It also emphasizes MATILDA-Online's potential as a transferable tool for supporting data-driven water resource management, regardless of the study region.

2 Study Site

The Kyzylsuu valley in the Tian Shan mountains is located in the Issyk-Kul district of Kyrgyzstan (see figure 1). The valley's first glaciological and meteorological records date back to the 1950s (WGMS, 2022). However, the first weather station, installed in 1957, was abandoned in the 1990s, and its records could not be accessed. A semi-automated weather station was

https://doi.org/10.5194/egusphere-2025-3462
Preprint. Discussion started: 17 November 2025

installed in 2007 and provided continuous observations from 2008 to 2017. The longest discharge record (1989-2020) comes from a station located near the valley entrance, about 25 km from the confluence of the Kyzylsuu River with Lake Issyk-Kul. It is mostly unaffected by irrigation diversions. On average, July has been the month of peak runoff in recent decades, when the maxima of precipitation and temperature, and thus melt, coincide. Although 10.8 % of the Kyzylsuu catchment is covered by glaciers, only the Kara-Batkak glacier (ID: RGI60-13.06359, RGI Consortium 2017) has long-term continuous mass balance observations (1957-1998 and since 2014, WGMS 2022). Table 1 summarizes the catchment's characteristics upstream of the gauging location.

3 Methods

MATILDA is forced with aggregated ERA5-Land reanalysis data (Muñoz Sabater et al., 2021) for calibration and an ensemble of NEX-GDDP-CMIP6 data (Thrasher et al., 2022) in two Shared Socioeconomic Pathways (SSP2 and SSP5) for the projections. Both climate forcing datasets and the digital elevation model were accessed via Google Earth Engine (GEE, Gorelick et al. 2017). Table A1 provides an overview of all used data sources. Details on preprocessing and bias adjustement can be found in Part 1 (Schuster et al., 2025c). Most of the processing chain for the present study, including the applied data, is documented in the MATILDA-Online Jupyter Book (https://matilda-online.github.io/jbook) and can be reproduced locally or in the cloud. However, the resource-intensive tasks of statistical parameter optimization, sensitivity testing, and uncertainty analysis were computed using parallel processing on a high-performance cluster (HPC) running Rocky Linux 8.6. While the calibration strategy needs to be tailored to the specific use case, study site, and technical capabilities of the user, the outlined procedure can provide a template for other melt-dominated catchments.

3.1 Calibration

Snow and glacier melt are the most important stream runoff contributors in most high mountain catchments (Woo and Thorne, 2006; Penna et al., 2014; Armstrong et al., 2018; Shannon et al., 2023). For an appropriate process representation in a conceptual model, it is crucial to integrate glacier surface mass balance (SMB) and snow data in addition to runoff (Duethmann et al., 2014; Finger et al., 2015; Nemri and Kinnard, 2020; van Tiel et al., 2020). Consequently, a four-step hierarchical process-based calibration approach was employed, integrating three calibration variables and multiple data sources.

3.1.1 Calibration Data

The availability of snow, glacier, and discharge data determined the calibration period as 2000-2020. The discharge data provided by the Kyrgyz HydroMet service was quality checked by the Central Asian Insitute for Applied Geosciences (CAIAG) yielding 17 years of daily values for calibration.

Due to their large uncertainty bands, all available SMB records were considered (Fig. 2). MATILDA's default SMB data from Shean et al. (2020) (2000–2018) averaged -0.156±0.324 m w.e. a^{-1} over all 38 glaciers. For 2000–2020 Hugonnet et al. (2021) estimated -0.462±0.175 m w.e. a^{-1}. Barandun et al. (2021) provided annual SMBs (-0.43 m w.e. a^{-1} for 2000–2018) for

https://doi.org/10.5194/egusphere-2025-3462
Preprint. Discussion started: 17 November 2025

the 7 largest glaciers (79.5% of glacier area) based on a combination of transient snowlines, geodetic surveys, and modeling. Miles et al. (2021) estimated -0.379 m w.e. a^{-1} from 2000–2016 for the same glaciers via remote sensing. The catchment's only in-situ observations are annual (1957–1998, 2014–2021) and seasonal (1976–1998, 2014–2021) SMB WGMS (2022) for Kara-Batkak glacier (-0.704 m w.e. a^{-1} for 2014–2021). Because of their qualitative approach, Barandun et al. (2021) was selected as the reference, while allowing for tolerance to account for the variety of observations (see 2).

The snow routine was calibrated using the High Mountain Asia Daily Snow Reanalysis (HMASR) dataset by Liu et al. (2021a) (Schuster et al., 2025c). The ensemble mean snow water equivalent (SWE) for 2000–2017 was reprojected to 16arcsec and clipped to catchment outlines following Gascoin (2021). As suggested by Liu et al. (2021b), only pixels classified as 'seasonal snow' were used, as this is where the method is most robust, due to the strong signal of disappearing snow in remote sensing data. While the excluded pixels largely correspond to glacierized areas, the differing resolutions of the datatsets (500m rasters vs. vector glacier outlines) result in a minor area discrepancy. To match the reference area of the SWE values before comparison, a scaling factor is applied to the simulated data during calibration.

The simulated and observed mean annual SMB are compared using the mean absolute error (MAE_{smb}). Both runoff (KGE_r) and SWE (KGE_{swe}) calibration use the Kling-Gupta Efficiency coefficient (Gupta and Kling, 2011; Kling et al., 2012).

3.1.2 Calibration Procedure

Steps 1-3 target water balance parameters in descending order of sensitivity. Step 4 calibrates all parameters that govern runoff timing. Table 2 summarizes the algorithms and criteria for the individual steps. The sample sizes N_{max} for all Latin Hypercube Samplings (LHS, McKay et al. 1979) were determined as

$$N_{max} = (k!)^{p-1}, \tag{1}$$

where k is the number of divisions per parameter and p is the number of parameters (Houska et al., 2023).

Step 1 - Input Correction: Three HBV parameters adjust input data for precipitation, snowfall, and evaporation, respectively, to account for observational errors. However, these adjustments may mask internal model uncertainties (Schuster et al., 2025c). Therefore, snowfall and evaporation correction were disabled (SFCF=1, CET=0). To calibrate the most sensitive parameter PCORR, the remaining 19 parameters were split into two subsets: (1) parameters governing the water balance, and (2) those controlling runoff timing, with the latter fixed on defaults. The stratified random samples (LHS) were filtered by all three objective functions (MAE_{smb}, KGE_{swe}, and KGE_r) and PCORR fixed on the posterior mean.

Step 2 - Snow Routine: The low-sensitivity parameters that impact the snow routine were set to the posterior means of step 1 (lr_{temp}, lr_{prec}) or the default (CFR). The remaining snow parameters (TT_{snow}, TT_{diff}, CFMAX_{snow}) were calibrated via LHS, filtered by KGE_{swe}, and set to posterior means.

Step 3 - Glacier Routine: The ice melt rate (CFMAX_{rel}) was constrained with uniform, stratified random samples and a target mean annual SMB as a compromise between different datasets (see 5.1.3). To account for the high source uncertainties, CFMAX_{rel} was constrained to the range where $\text{MAE}_{smb} < 100$ mm.

https://doi.org/10.5194/egusphere-2025-3462
Preprint. Discussion started: 17 November 2025

Step 4 - Soil, Response, and Routing: The remaining 11 parameters were calibrated using the Differential Evolution Markov Chain algorithm DEMCz (ter Braak and Vrugt, 2008). This technique is more efficient than other Monte Carlo Markov Chain (MCMC) algorithms at finding global optima and does not require prior distribution information (Braak, 2006; ter Braak and Vrugt, 2008; Turner et al., 2013). However, it requires one explicit objective function, and is sensitive to the settings and likelihood function used (Houska et al., 2015). The KGE, as an informal likelihood function, can cause problems with MCMC techniques due to negative values and high proposal acceptance rates (Mantovan and Todini, 2006; Stedinger et al., 2008; Liu et al., 2022). To mitigate these problems, we employed the gamma-distribution-based KGE version proposed by Liu et al. (2022). Once all chains fulfilled the Gelman-Rubin convergence criterion (Gelman and Rubin, 1992), the sample set was filtered using an MAE_{smb} threshold as well as seasonal ($\text{KGE}_{r,s}$ for Apr-Sep; $\text{KGE}_{r,w}$ for Oct-Mar) and total KGE_r criteria.

3.2 Validation

Due to gaps of up to 2.5 years in the discharge data, validation focused on 2018–2020 using a split-sample approach. Relative glacier area changes during calibration were estimated via Landsat 7 (25.08.2002) and Sentinel-2 (21.07.2022) scenes using the GEE Random Forest glacier mapping workflow of Ali et al. (2023).

We also compared our results with Chevallier et al. (2023), who simulated the Kyzylsuu catchment until 2060 using the distributed HDSM model (Savéan et al., 2015). The study used the same reanalysis data, but bias-adjusted to additional stations, for calibration and the CNRM-CM6-1 model for projections (Voldoire et al., 2019). Therefore, we extracted the CNRM-CM6-1 runs from our ensemble to compare simulated changes between 2011-2020 and 2051-2060 with the reference study. However, Chevallier et al. (2023) applied quantile mapping based on only six years (2015–2020) of station data, with unclear trend preservation. Their snow routine was calibrated to remote sensing snow cover data and the glacier routine calibration focused on Kara-Batkak glacier only while glacier evolution was neglected.

3.3 Uncertainty analysis

To assess evolving parameter uncertainty during calibration, 20'000 random samples were computed for five calibration stages: **(a)** all parameters open (21 parameters), **(b)** correction factors fixed (18), **(c)** after snow calibration (12), **(d)** after glacier calibration (11), **(e)** all values of (d) where $\text{KGE}_r > 0.8$. The hydrograph ranges for (a–d) illustrate parameter uncertainty.

The uncertainty in glacier evolution due to calibration data inconsistencies was assessed by forcing the model with the full range of ice melt rates supported by the literature. The lower bound was set using the highest SMB from Shean et al. (2020) (-0.156 m w.e. a^{-1}, 2000–2018), the upper bound using the SMB of Karabatkak Glacier from 2014–2020 (WGMS, 2022), as used by Chevallier et al. (2023) (-0.704 m w.e. a^{-1}). The model was run with melt rates ranging from the upper to the lower bound in 5 % increments under both SSP scenarios.

https://doi.org/10.5194/egusphere-2025-3462
Preprint. Discussion started: 17 November 2025

4 Results

4.1 Reanalysis data

ERA5-Land air temperature agrees well with the local weather station data. However, precipitation is substantially overestimated as reflected by the total summer precipitation (Apr–Sep). Where ERA5-Land estimated a total of 9590 mm from 2008–2017 in the Kyzylsuu catchment, only 4330 mm w.e. were observed – an overestimation of 108±62%. To some extent, this can be attributed to the 'constant drizzle' issue in climate models (He et al., 2019; Chiaravalloti et al., 2022) as highlighted by the strong underestimation of days without precipitation (ERA5L: 4.2% vs. Obs: 72.2%).

4.2 Calibration

Table 2 summarizes all calibration steps and final parameters. Each of the following steps refers to one column in the table.

Step 1 - Input Correction: To determine PCORR, the LHS results were filtered for $\text{MAE}_{smb} < 100$ mm and $\text{KGE}_{swe} > 0.7$. The top 10% ($0.46 < \text{KGE}_r < 0.55$) were selected. Posterior distributions were mostly Gaussian, with some skewness or bimodality (see Figure A11). PCORR was fixed at the posterior mean of 0.58, as 68% of all values were within ±0.04.

Step 2 - Snow Routine: A scaling factor of 0.928 was applied to address the coarser resolution of the mask for seasonal snow (see 3.1.1). Samples with $\text{KGE}_{swe} > 0.8$ (n=29) were retained. All parameters showed Gaussian distributions and were fixed at posterior means.

Step 3 - Glacier Melt Rate: Excluding samples with $\text{MAE}_{smb} > 100$ mm constrained CFMAX_{rel} to 1.20–1.53, corresponding to 4.04–5.16 mm K^{-1} d^{-1}.

Step 4 - Soil and Routing: DEMCz sampling converged after 85,400 iterations. The final selection ($\text{MAE}_{smb} < 50$ mm) yielded KGE_r = 0.88, with seasonal values of 0.88 ($\text{KGE}_{r,s}$) and 0.24 ($\text{KGE}_{r,w}$).

4.3 Validation

The remote sensing analysis shows glacier area declined from 39.2 km^2 (2002, Landsat 7) to 31.9 km^2 (2022, Sentinel-2) – a loss of 18.6%. The simulated area dropped from 31.8 km^2 (2000) to 28.1 km^2 (2020), or 11.7%. However, the Random Forest approach estimates the inital glacier area to be 23.3 % (7.4 km^2) larger then in the RGI6, which also refers to 2002 (see Figure A13). The full discharge time series and runoff contributions from 2000–2020 along with average annual cycles are shown in Figure 3. Runoff validation yielded KGE_r = 0.89 (NSE = 0.83, RMSE = 21.0 mm) during calibration and 0.88 (NSE = 0.84, RMSE = 20.6 mm) during validation. Figure 4 compares the simulated average annual SWE cycle with observations, showing KGE_{swe} = 0.81 (MAE = 24.4 mm, RMSE = 36.0 mm) for calibration. No SWE data were available for the validation period. Mean annual SMB during calibration was -0.44 m w.e. Simulated SMB is within uncertainty bands of the long-term remote sensing datasets (Shean et al., 2020; Miles et al., 2021; Hugonnet et al., 2021), though annual records vary.

https://doi.org/10.5194/egusphere-2025-3462
Preprint. Discussion started: 17 November 2025

4.4 Projections

4.4.1 Bias Adjustment

Of the 34 CMIP6 ensemble models provided via GEE, three failed the consistency checks (Schuster et al., 2025c). A list of the final ensemble members can be found in table A2. Figures A1 to A4 show the remaining models before and after bias adjustment. Both SSP scenarios show positive temperature trends, while precipitation remains relatively constant (see Figures A5 and A6). The bias-adjusted data shows high agreement with the target data for temperature (R^2 between 0.86 and 0.9) in both scenarios, and moderate agreement for monthly precipitation (R^2 between 0.35 and 0.6) as visualized in Figure A7 to A10 in the Appendix.

4.4.2 Climate Trends

Figure 6 summarizes projected changes in the water balance. Tables A3 and A4 in the Appendix present ensemble means and standard deviations for selected model outputs. All values hereafter refer to ensemble means. Trends are based on annual aggregates whereas relative changes refer to means of the first and last decade of the century. Unless noted, all trends are significant ($p< 0.01$). The annual mean temperature is projected to rise at 0.03 K a^{-1} for SSP2 and 0.06 K a^{-1} for SSP5, increasing potential evaporation by 35% and 76%. Actual evaporation rises by 16% (35%). Precipitation declines slightly with a linear trend of -0.7 mm/a in both scenarios, while it's seasonality remains stable, but with a systematic difference: CMIP6 models peak in June, while ERA5-Land peaks in July. The length and frequency of dry spells increase consistently, reaching up to 121 days per year by 2090–2100 (trend: 0.8 d/a).

4.4.3 Trends in Water Balance

The glacier area is projected to shrink by 90% (SSP2) and 99.8% (SSP5) between 2000 to 2100. The contribution of ice melt to runoff initially rises from 7.8% to over 12% (13%) by mid-century. Subsequently, it drops to 1.8% (0%) by the period 2091-2100. Total runoff declines by -1.6 mm/a (-1.9 mm/a), amounting to 18% (23%) less runoff over the final decade compared to the first. The snow amount remains stable under SSP2 (not significant trend: -0.02 mm/a) but drops by 0.50 mm/a under SSP5. The snowmelt fraction in ruoff rises in both scenarios from 41.1% (2000–2010) to 52.6% (SSP2) and 43.8% (SSP5) between 2090 and 2100. However, it declines after 2060 under SSP5. The melt season begins approx. one month earlier (SSP2: -20 days, SSP5: -44 days) and extends from 151 to 180 (209) days. The peak runoff shifts from late July (DoY 212) to late May (DoY 150, SSP2) or mid-May (DoY 136, SSP5).

4.5 Uncertainty

Figure 7 illustrates the evolving parameter uncertainty through model calibration. Because MATILDA is sensitive to external correction factors (Schuster et al., 2025c), step 1 has the strongest impact. Calibrating the snow module further narrows the parameter space, while constraining the ice melt rate has minimal effect after all snow parameters are calibrated. After applying

https://doi.org/10.5194/egusphere-2025-3462
Preprint. Discussion started: 17 November 2025

the KGE_r filter in the final step, little parameter uncertainty remains, despite 11 open parameters. While this is true for the calibration period, the ice melt rate strongly affects projections. Calibrating to the highest SMB estimate (Shean et al., 2020) yields a melt rate of 2.11 mm K^{-1} d^{-1}, while calibrating only to in-situ data of a single glacier returns 6.11 mm K^{-1} d^{-1}. Figure 8 illustrates the wide range of outcomes for three related variables. For example, depending on SMB data used, glaciers may disappear by 2084 under SSP5 or retain over 5 km^2 by 2100. Glacier runoff timing also varies significantly, and the peak runoff may already have past.

5 Discussion

When considering MATILDA's overall performance, two major sources of uncertainty must be taken into account: forcing data and the modeling workflow. Several product-specific uncertainties are addressed in related publications and are therefore not discussed here. However, some known issues directly impact this case study.

5.1 Data

5.1.1 Reanalysis data

As confirmed by our analysis for the observation period, ERA5-Land is known to overestimate precipitation in high mountains (Wu et al., 2023b). While seasonal patterns and peak timing are consistent, light rain and drizzle are often overestimated and extremes are underestimated (He et al., 2019; Chiaravalloti et al., 2022; Gomis-Cebolla et al., 2023). Although a precipitation correction factor can address this issue in long-term water balance projections, it cannot adjust for shortcomings in the representation of seasonal variations and extreme events. Other ERA5 uncertainties are well covered in existing literature (e.g., Hamm et al. 2020; Muñoz Sabater et al. 2021; Zhao and He 2022; Gomis-Cebolla et al. 2023). Regarding snow, however, the used SWE data was derived using Merra-2 forcing (Gelaro et al., 2017) at 0.5° by 0.625° resolution for the snow model ensemble (Liu et al., 2021a), which differs from ERA5-Land. As the ensemble was calibrated with remote sensing snow cover data, it served as a proxy for observations in this study. Differences from ERA5-Land precipitation were accounted for by including SWE data in the calibration of PCORR.

5.1.2 Climate scenarios

As a relatively new dataset, NEX-GDDP-CMIP6 lacks comprehensive performance assessments at regional and local levels. Nevertheless, some studies show it can outperform native CMIP6 data (Dioha et al., 2024) and provide good temperature estimates (Wu et al., 2023a), even in complex terrain (Zou et al., 2024). Precipitation trends in large catchments are also captured well (Jiang et al., 2023), though limitations remain in representing fluctuations (Wu et al., 2023a) and spatial precipitation patterns in mountains (Yuan et al., 2023). Aggregation may reduce some of these issues, but validation against observations remains essential. Figures A1 to A10 in the Appendix illustrate model performance before and after bias adjustment. The bias adjustment (Schuster et al., 2025c) performs well for both variables, with stronger agreement for temperature. Monthly precip-

https://doi.org/10.5194/egusphere-2025-3462
Preprint. Discussion started: 17 November 2025

itation distributions align with ERA5-Land, but totals above 250 mm show larger differences, partly due to known ERA5-Land biases in extremes. The final 31 CMIP6 models show high agreement in precipitation trends, resulting in narrow ensemble confidence intervals for total precipitation, snowmelt, and runoff. Qualitative ensemble selection (e.g. by specific process representation) can further improve robustness.

5.1.3 Observations

Runoff and SMB observations are subject to substantial uncertainty due to limited data quality and availability. Chevallier et al. (2023) questioned the reliability of the same runoff dataset used here, citing unclear measurement methods and the limited frequency of discharge observations. Historic SMB records often contain large gaps or were discontinued after 1990 (Hoelzle et al., 2017). Further, even longer records of single glaciers can bias glacier modeling. In the study catchment, Kara-Batkak loses mass faster than the catchment average by up to 16.3 % (Shean et al., 2020; Barandun et al., 2021; Miles et al., 2021), suggesting calibration on this single SMB time series may overestimate glacier melt. By contrast, remote sensing offers broad glacier coverage but mostly long-term average estimates. Compared to Barandun et al. (2021), MATILDA's default dataset (Shean et al., 2020) shows more positive SMBs for all seven glaciers ($\overline{\Delta} = 0.224 \pm 0.141$ m w.e.), with three exceeding uncertainty bounds, indicating underestimated mass loss. Although this highlights the value of multiple data sources, even combined datasets allow for a wide range of glaciation scenarios (Figure 8), which is a key driver of projection uncertainty. Additionally, most glacial datasets use 2000 as the reference year, limiting calibration despite the availability of longer discharge records.

5.2 Model Performance

5.2.1 Validation

Despite considerable uncertainties in all validation datasets, MATILDA performs well across most objectives. During validation, runoff closely matches observations, though peak flows are less accurately captured than in calibration. Both periods show a consistent delay in spring runoff onset and fall recession, with low flows generally underestimated (Figure 3). Simulated glacier SMB falls within the range of all datasets used, though none of the intra-annual variations match (Figure 2). Changes in glacier area align well with remote-sensing estimates when the overestimation in 2002 is accounted for. The mean annual SWE cycle is reproduced on average (Figure 4) but MATILDA overestimates SWE maxima and underestimates minima, since the catchment scale cannot resolve spatial variability in snowmelt. Separation into sub-catchments to account for spatial variability of air temperature and radiation input may improve the representation of snow cover seasonality but increases processing time.

5.2.2 Climate Change Signals

The observed trends are consistent with earlier studies in high mountain catchments, suggesting a shift from a glacial-nival to a nival-pluvial runoff regime (Braun and Hagg, 2009; Sorg et al., 2012; Li et al., 2020). Simulation trends, and the fact that 1991–2000 (846.2 mm/a) and 2000–2010 (854.5 mm/a) had the highest average precipitation of all simulated decades, indicate peak runoff around the millennium, followed by a decline in glacial runoff and total streamflow in both scenarios (Milner

https://doi.org/10.5194/egusphere-2025-3462
Preprint. Discussion started: 17 November 2025

et al., 2009; Shea et al., 2013; Hock et al., 2019). However, the buffering role of meltwater during dry seasons noted in other studies (Armstrong et al., 2018; Pritchard, 2019; Barandun et al., 2020; Van Tiel et al., 2021; Barandun et al., 2021) is less evident, since peak evaporation and precipitation typically coincide. Nevertheless, reduced meltwater decreases peak runoff and impairs the ability to offset increasing dry spells, especially in late summer and fall. Despite this, the expected earlier onset of spring runoff and summer peak flow (Barnett et al., 2005; Hock et al., 2019) is consistent with simulations for the nearby Naryn catchment (Schaffhauser et al., 2023; Shannon et al., 2023) and other regional studies (Sorg et al., 2012; Kriegel et al., 2013; Chen et al., 2018; Barandun et al., 2020; Siegfried et al., 2024).

5.2.3 Result Comparison

Validation against Chevallier et al. (2023) revealed significant discrepancies in the adjusted forcing and the simulations. Our results indicate stronger warming from the second to sixth decade: 1.87,°C for SSP2 (SSP5: 2.63,°C) vs. 0.77,°C (1.77,°C) in Chevallier et al. (2023), and a higher E_{pot} increase of 20.2 % (29.2 %) vs. 2 % (6.5 %). The variability of precipitation is similar, but the annual totals are about 10% higher in our case. All simulated water balance components (2011–2020) are higher in Chevallier et al. (2023), with minor differences in snowmelt (factor 1.6) and E_{act} (1.7). However, glacier melt is 5.3 times higher—though flagged as an overestimation due to their static glacier assumption. Nevertheless, the trends in E_{act} align: 7.3 % (12.7 %) vs. 3.3 % (13 %), while snowmelt trends diverge: +16.3 % (11.3 %) in our results vs. -9.5 % (-17.5 %) in theirs. These differences can mainly be attributed to the different model setups, including distinct bias adjustments, and our use of the highly temperature-sensitive method by Oudin et al. (2005) to estimate evaporation compared to the Penman-Monteith method of Allan et al. (1998). Additionally, Chevallier et al. (2023) only report decadal means, not trends, and SWE differences after 2020 are minor, suggesting discrepancies in their calibration data for 2010–2020. Ice melt and total runoff estimates remain incomparable due to their static glacier scheme, in which ice melt even surpasses snow melt in the projection.

The comparison of two approaches forced by the same original climate data illustrates the importance of carefully selecting the bias adjustment approach and the target data. The use of a downscaled CMIP6 product and trend-preserving bias adjustment to ERA5-Land results in significantly higher temperature and precipitation trends. By contrast, meteorological observations as used by Chevallier et al. (2023) generally provide valuable insights into local conditions, but often suffer from low spatial and temporal coverage and quality shortcomings (Xenarios et al., 2019) such as unquantified precipitation undercatch (Kochendorfer et al., 2017). Moreover, the disparate SWE simulations demonstrate the impact of the chosen snow calibration approach on the simulated water balance. Dedicated snow reanalysis products have advantages over snow cover area data alone, especially regarding peak snow storage (Liu et al., 2021b).

5.2.4 Limitations and Opportunities

Though there are few observations in many target regions, several global datasets could improve MATILDA's predictive power by addressing current calibration limitations. Soil and groundwater parameters remain uncalibrated with explicit data, so the final calibration step is determined by compensating soil and routing parameters. However, datasets like HiHydroSoil v2.0 (Simons et al., 2020), accessible via GEE, require expert adaptation to HBV parameters. Furthermore, land degradation result-

https://doi.org/10.5194/egusphere-2025-3462
Preprint. Discussion started: 17 November 2025

ing from climate change and overgrazing poses an evident risk in Central Asia affecting evaporation and soil properties (Chen et al., 2019). In contrast, high-altitude greening due to rising temperatures increases evapotranspiration (Mastrotheodoros et al., 2020; Yang et al., 2020). Such dynamic changes cannot be represented with static parameters which is a key limitation of conceptual models (Duethmann et al., 2020). CMIP6 models incorporate land cover change, but at a large scale (Lawrence et al., 2016; Ma et al., 2020). More impact oriented datasets like those of the Inter-Sectoral Impact Model Intercomparison Project (ISIMIP, Warszawski et al. 2014; Frieler et al. 2017; Lange 2019) can add value, but their coarse resolution ($\geq$0.5°) and complexity require complex downscaling and preprocessing, limiting their integration into MATILDA-Online without additional resources.

6 Conclusions

Public datasets with broad temporal and spatial coverage can help address data scarcity in regions like Central Asia. Yet, limited access to data and models remains a major barrier for local users. Many global and regional tools lack the resolution for reliable long-term water balance estimates in mesoscale catchments and require intensive downscaling and technical expertise. MATILDA offers a solution by supporting, educating, and empowering water management stakeholders in regions affected by climate change. In the demonstrated setup, MATILDA has shown reliable performance in simulating key hydrological components across different periods and scenarios. Iterative assessment of parameter uncertainty has shown that robust calibration of water balance parameters is essential, while the impact of most soil and routing parameters is less significant in the long term. MATILDA has proven to effectively capture general seasonal patterns and trends in the water balance. Projections for the Kyzylsuu catchment indicate a significant increase in evapotranspiration, a reduction in glacier mass of up to 99%, and a shift toward earlier spring runoff and summer peak runoff. These changes are consistent with trends observed in other catchments in HMA, although the exact runoff contributions vary among related studies.

Despite these promising results, significant uncertainties remain. As a lumped conceptual model, MATILDA does not account for spatial variability in forcing data and related processes, resulting in temporal inaccuracies. Further subdivision into smaller sub-catchments may address this, particularly the timing of snowmelt, but increases processing costs. In addition, the model's static parameters cannot account for dynamic trends associated with land surface changes. However, most of the projection uncertainty is associated with biases in the precipitation data and the observations used for calibration. The temperature index model with the modified Δh routine can provide reasonable long-term estimates of glacial contributions to runoff, including stabilizing effects at higher elevations (Schuster et al., 2025c). However, this setup fails to reproduce observed inter-annual changes and neglects important glaciological factors such as glacier dynamics and debris cover. While a more comprehensive glacier model could address some of these limitations, the greatest uncertainty in glaciation scenarios arises from inconsistencies in the mass balance datasets used as reference. Therefore, despite the improving quality of model-based datasets, the availability and reliability of observations are essential for predicting water balance and runoff contributions.

https://doi.org/10.5194/egusphere-2025-3462
Preprint. Discussion started: 17 November 2025

Code and data availability. The MATILDA core model and calibration module are published as a Python package (Schuster et al., 2025b). MATILDA-Online is available as a repository (Schuster et al., 2025a) and deployed as a Jupyter Book on the MATILDA-Online website (https://matilda-online.github.io/jbook). All modeling results, forcing datasets, and discharge observations are available as example datasets or can be reproduced by running the workflow locally or online. All other data can be accessed from the original sources cited in the text and listed in Table A1.

Author contributions. A. Osmonov, C. Schneider, and P. Schuster obtained funding and developed the study concept. A. Osmonov acquired and digitized the discharge and meteorological data. P. Schuster and A. Georgi collected all cloud-based datasets and designed the Jupyter Book featured on the MATILDA Online website. P. Schuster and T. Sauter developed the calibration approach. P. Schuster also gathered all glaciological data, performed the model calibration, ran the projections, conducted the data analysis, and prepared the manuscript, including all figures. A. Osmonov, P. Schuster, and A. Georgi carried out result validation. All authors contributed to discussions on processing steps and interpreting results. A. Osmonov, P. Schuster, and A. Georgi carried out result validation. All authors contributed to discussions on processing steps and interpreting results. C. Schneider and T. Sauter supervised the work and assisted in editing the final paper.

Competing interests. The authors declare that the research was conducted in the absence of any commercial or financial relationships that could be construed as a potential conflict of interest.

Acknowledgements. A. Osmonov initially conducted research at the study site as part of an International Climate Protection Fellowship from the Alexander von Humboldt Foundation (reference KGZ 1208824 IKS). Subsequent work was funded by Humboldt-Universität zu Berlin. The authors would like to thank Bakyt Ermenbaev and the Hydro-Meteorological Service under the Ministry of Emergency Situations of the Kyrgyz Republic (Kyrgyz HydroMet) for providing the discharge and meteorological observations. We would also like to thank Mia Janzen for her assistance in maintaining MATILDA-Online.

The following AI tools were used for preparing this manuscript: Consensus.app (https://consensus.app) for literature research, NotebookLM by Google (https://notebooklm.google) for literature summaries, DeepL Write (https://www.deepl.com/write) and ChatGPT 4o (https://openai.com/chatgpt) for grammar and spelling checks, and text shortening, ChatGPT 4o for LaTeX and figure editing, and Midjourney (https://www.midjourney.com) for the original draft of the "cupcake" figure used in the graphical abstract.

https://doi.org/10.5194/egusphere-2025-3462
Preprint. Discussion started: 17 November 2025

References

Aggarwal, A., Frey, H., McDowell, G., Drenkhan, F., Nüsser, M., Racoviteanu, A., and Hoelzle, M.: Adaptation to climate change induced water stress in major glacierized mountain regions, Climate and Development, 14, 665–677, https://doi.org/10.1080/17565529.2021.1971059, 2022.

Aizen, V. B., Aizen, E. M., and Melack, J. M.: CLIMATE, SNOW COVER, GLACIERS, AND RUNOFF IN THE TIEN SHAN, CENTRAL ASIA1, JAWRA Journal of the American Water Resources Association, 31, 1113–1129, https://doi.org/https://doi.org/10.1111/j.1752-1688.1995.tb03426.x, 1995.

Aizen, V. B., Aizen, E. M., and Melack, J. M.: Precipitation, melt and runoff in the northern Tien Shan, Journal of Hydrology, 186, 229–251, https://doi.org/https://doi.org/10.1016/S0022-1694(96)03022-3, 1996.

Aizen, V. B., Aizen, E. M., Melack, J. M., and Dozier, J.: Climatic and Hydrologic Changes in the Tien Shan, Central Asia, Journal of Climate, 10, 1393 – 1404, https://doi.org/https://doi.org/10.1175/1520-0442(1997)010<1393:CAHCIT>2.0.CO;2, 1997.

Ali, A., Dunlop, P., Coleman, S., Kerr, D., McNabb, R., and Noormets, R.: Glacier area changes in Novaya Zemlya from 1986–89 to 2019–21 using object-based image analysis in Google Earth Engine, Journal of Glaciology, 69, 1–12, https://doi.org/10.1017/jog.2023.18, 2023.

Allan, R., Pereira, L., and Smith, M.: Crop evapotranspiration-Guidelines for computing crop water requirements-FAO Irrigation and drainage paper 56, 56, 1–15, 1998.

Armstrong, R. L., Rittger, K., Brodzik, M. J., Racoviteanu, A., Barrett, A. P., Khalsa, S.-J. S., Raup, B., Hill, A. F., Khan, A. L., Wilson, A. M., Kayastha, R. B., Fetterer, F., and Armstrong, B.: Runoff from glacier ice and seasonal snow in High Asia: separating melt water sources in river flow, Regional Environmental Change, 19, 1249–1261, https://doi.org/10.1007/s10113-018-1429-0, 2018.

Barandun, M., Fiddes, J., Scherler, M., Mathys, T., Saks, T., Petrakov, D., and Hoelzle, M.: The state and future of the cryosphere in Central Asia, Water Security, 11, 100 072, https://doi.org/https://doi.org/10.1016/j.wasec.2020.100072, 2020.

Barandun, M., Pohl, E., Naegeli, K., McNabb, R., Huss, M., Berthier, E., Saks, T., and Hoelzle, M.: Hot Spots of Glacier Mass Balance Variability in Central Asia, Geophysical Research Letters, 48, e2020GL092 084, https://doi.org/https://doi.org/10.1029/2020GL092084, e2020GL092084 2020GL092084, 2021.

Barnett, T. P., Adam, J. C., and Lettenmaier, D. P.: Potential impacts of a warming climate on water availability in snow-dominated regions, Nature, 438, 303–309, https://doi.org/10.1038/nature04141, 2005.

Bernauer, T. and Siegfried, T.: Climate change and international water conflict in Central Asia, Journal of Peace Research, 49, 227–239, https://doi.org/10.1177/0022343311425843, 2012.

Bocchiola, D., Pelosi, M. G., and Soncini, A.: Effects of hydrological changes on cooperation in transnational catchments: the case of the Syr Darya, Water International, 42, 852–873, https://doi.org/10.1080/02508060.2017.1376568, 2017.

Bolch, T.: Climate change and glacier retreat in northern Tien Shan (Kazakhstan/Kyrgyzstan) using remote sensing data, Global and Planetary Change, 56, 1–12, https://doi.org/https://doi.org/10.1016/j.gloplacha.2006.07.009, climate Change Impacts on Mountain Glaciers and Permafrost, 2007.

Bolch, T., Marchenko, S., Braun, L. N., Hagg, W., Severskiy, I. V., and Young, G.: Significance of glaciers, rockglaciers and ice-rich permafrost in the Northern Tien Shan as water towers under climate change conditions, IHP/HWRP-Berichte, pp. 132–144, 2009.

Braak, C.: A Markov Chain Monte Carlo version of the genetic algorithm Differential Evolution: easy Bayesian computing for real parameter spaces, Statistics and Computing, 16, 239–249, https://doi.org/10.1007/s11222-006-8769-1, 2006.

https://doi.org/10.5194/egusphere-2025-3462
Preprint. Discussion started: 17 November 2025

Braun, L. and Hagg, W.: Present and future impact of snow cover and glaciers on runoff from mountain regions – comparison between Alps and Tien Shan, vol. 8, pp. 36–43, ISBN 1614-1180, 2009.

Chen, T., Bao, A., Jiapaer, G., Guo, H., Zheng, G., Jiang, L., Chang, C., and Tuerhanjiang, L.: Disentangling the relative impacts of climate change and human activities on arid and semiarid grasslands in Central Asia during 1982-2015, The Science of the Total Environment, 653, 1311–1325, https://doi.org/10.1016/j.scitotenv.2018.11.058, 2019.

Chen, Y., Li, W., Deng, H., Fang, G., and Li, Z.: Changes in Central Asia's Water Tower: Past, Present and Future, Scientific Reports, 6, 35 458, https://doi.org/10.1038/srep35458, 2016.

Chen, Y., Li, Z., Fang, G., and Li, W.: Large Hydrological Processes Changes in the Transboundary Rivers of Central Asia, Journal of Geophysical Research: Atmospheres, 123, 5059–5069, https://doi.org/https://doi.org/10.1029/2017JD028184, 2018.

Chevallier, P., Satylkanov, R., Delclaux, F., Gascoin, S., Ermenbaev, B., and Crétaux, J.-F.: Current and future water balance of a mountain subcatchment of Issyk-Kul Lake, Tien Shan range, Kyrgyzstan, Science of The Total Environment, 897, 165 363, https://doi.org/10.1016/j.scitotenv.2023.165363, 2023.

Chiaravalloti, F., Caloiero, T., and Coscarelli, R.: The Long-Term ERA5 Data Series for Trend Analysis of Rainfall in Italy, Hydrology, 9, https://doi.org/10.3390/hydrology9020018, 2022.

De Stefano, L., Petersen-Perlman, J. D., Sproles, E. A., Eynard, J., and Wolf, A. T.: Assessment of transboundary river basins for potential hydro-political tensions, Global Environmental Change, 45, 35–46, https://doi.org/https://doi.org/10.1016/j.gloenvcha.2017.04.008, 2017.

Dickich, A. and Hagg, W.: Climate driven changes of glacier runoff in the Issyk-Kul basin, Kyrgyzstan, Zeitschrift für Gletscherkunde und Glazialgeologie, 39, 75–86, 2004.

Dioha, E. C., Chung, E.-S., Ayugi, B. O., Babaousmail, H., and Sian, K. T. C. L. K.: Quantifying the Added Value in the NEX-GDDP-CMIP6 Models as Compared to Native CMIP6 in Simulating Africa's Diverse Precipitation Climatology, Earth Systems and Environment, 8, 417–436, https://doi.org/10.1007/s41748-024-00397-x, 2024.

Duethmann, D., Peters, J., Blume, T., Vorogushyn, S., and Güntner, A.: The value of satellite-derived snow cover images for calibrating a hydrological model in snow-dominated catchments in Central Asia, Water Resources Research, 50, 2002–2021, https://doi.org/10.1002/2013WR014382, 2014.

Duethmann, D., Blöschl, G., and Parajka, J.: Why does a conceptual hydrological model fail to correctly predict discharge changes in response to climate change?, Hydrology and Earth System Sciences, 24, 3493–3511, https://doi.org/10.5194/hess-24-3493-2020, 2020.

Farinotti, D., Longuevergne, L., Moholdt, G., Duethmann, D., Mölg, T., Bolch, T., Vorogushyn, S., and Güntner, A.: Substantial glacier mass loss in the Tien Shan over the past 50 years, Nature Geoscience, 8, 716–722, 2015.

Farinotti, D., Huss, M., Fürst, J. J., Landmann, J., Machguth, H., Maussion, F., and Pandit, A.: A Consensus Estimate for the Ice Thickness Distribution of All Glaciers on Earth, Nature Geoscience, 12, 168–173, https://doi.org/10.1038/s41561-019-0300-3, 2019.

Finger, D., Vis, M., Huss, M., and Seibert, J.: The value of multiple data set calibration versus model complexity for improving the performance of hydrological models in mountain catchments, Water Resources Research, 51, 1939–1958, https://doi.org/https://doi.org/10.1002/2014WR015712, 2015.

Frieler, K., Lange, S., Piontek, F., Reyer, C. P. O., Schewe, J., Warszawski, L., Zhao, F., Chini, L., Denvil, S., Emanuel, K., Geiger, T., Halladay, K., Hurtt, G., Mengel, M., Murakami, D., Ostberg, S., Popp, A., Riva, R., Stevanovic, M., Suzuki, T., Volkholz, J., Burke, E., Ciais, P., Ebi, K., Eddy, T. D., Elliott, J., Galbraith, E., Gosling, S. N., Hattermann, F., Hickler, T., Hinkel, J., Hof, C., Huber, V., Jägermeyr, J., Krysanova, V., Marcé, R., Müller Schmied, H., Mouratiadou, I., Pierson, D., Tittensor, D. P., Vautard, R., van Vliet, M., Biber, M. F., Betts, R. A., Bodirsky, B. L., Deryng, D., Frolking, S., Jones, C. D., Lotze, H. K., Lotze-Campen, H., Sahajpal, R., Thonicke,

https://doi.org/10.5194/egusphere-2025-3462
Preprint. Discussion started: 17 November 2025

K., Tian, H., and Yamagata, Y.: Assessing the impacts of 1.5 °C global warming – simulation protocol of the Inter-Sectoral Impact Model Intercomparison Project (ISIMIP2b), Geoscientific Model Development, 10, 4321–4345, https://doi.org/10.5194/gmd-10-4321-2017, 2017.

Gascoin, S.: Snowmelt and Snow Sublimation in the Indus Basin, Water, 13, https://doi.org/10.3390/w13192621, 2021.

Gelaro, R., McCarty, W., Suárez, M. J., Todling, R., Molod, A., Takacs, L., Randles, C. A., Darmenov, A., Bosilovich, M. G., Reichle, R., et al.: The Modern-Era Retrospective Analysis for Research and Applications, Version 2 (MERRA-2), Journal of Climate, 30, 5419–5454, 2017.

Gelman, A. and Rubin, D. B.: Inference from Iterative Simulation Using Multiple Sequences, Statistical Science, 7, 457–472, http://www.jstor.org/stable/2246093, 1992.

Gerlitz, L., Vorogushyn, S., and Gafurov, A.: Climate informed seasonal forecast of water availability in Central Asia: State-of-the-art and decision making context, Water Security, 10, 100 061, https://doi.org/https://doi.org/10.1016/j.wasec.2020.100061, 2020.

Gomis-Cebolla, J., Rattayova, V., Salazar-Galán, S., and Francés, F.: Evaluation of ERA5 and ERA5-Land reanalysis precipitation datasets over Spain (1951–2020), Atmospheric Research, 284, 106 606, https://doi.org/https://doi.org/10.1016/j.atmosres.2023.106606, 2023.

Gorelick, N., Hancher, M., Dixon, M., Ilyushchenko, S., Thau, D., and Moore, R.: Google Earth Engine: Planetary-scale geospatial analysis for everyone, Remote Sensing of Environment, 202, 18–27, https://doi.org/https://doi.org/10.1016/j.rse.2017.06.031, big Remotely Sensed Data: tools, applications and experiences, 2017.

Gupta, H. V. and Kling, H.: On typical range, sensitivity, and normalization of Mean Squared Error and Nash-Sutcliffe Efficiency type metrics, Water Resources Research, 47, https://doi.org/https://doi.org/10.1029/2011WR010962, 2011.

Hagg, W., Braun, L., Kuhn, M., and Nesgaard, T.: Modelling of hydrological response to climate change in glacierized Central Asian catchments, Journal of Hydrology, 332, 40–53, https://doi.org/https://doi.org/10.1016/j.jhydrol.2006.06.021, 2007.

Hamm, A., Arndt, A., Kolbe, C., Wang, X., Thies, B., Boyko, O., Reggiani, P., Scherer, D., Bendix, J., and Schneider, C.: Intercomparison of Gridded Precipitation Datasets over a Sub-Region of the Central Himalaya and the Southwestern Tibetan Plateau, Water, 12, https://doi.org/10.3390/w12113271, 2020.

He, S., Yang, J., Bao, Q., Wang, L., and Wang, B.: Fidelity of the Observational/Reanalysis Datasets and Global Climate Models in Representation of Extreme Precipitation in East China, Journal of Climate, 32, 195 – 212, https://doi.org/https://doi.org/10.1175/JCLI-D-18-0104.1, 2019.

Hock, R., Rasul, G., Adler, C., Caceres, B., Gruber, S., Hirabayashi, Y., Jackson, M., Kääb, A., Kang, S., Kutuzov, S., Milner, A., Molau, U., Morin, S., Orlove, B., Steltzer, H., Allen, S., Arenson, L., Baneerjee, S., Barr, I., Bórquez, R., Brown, L., Cao, B., Carey, M., Cogley, G., Fischlin, A., de Sherbinin, A., Eckert, N., Geertsema, M., Hagenstad, M., Honsberg, M., Hood, E., Huss, M., Zamora, E. J., Kotlarski, S., Lefeuvre, P., Moreno, J. I. L., Lundquist, J., McDowell, G., Mills, S., Mou, C., Nepal, S., Noetzli, J., E, P., Pepin, N., Rixen, C., Shahgedanova, M., Skiles, S. M., Vincent, C., Viviroli, D., Weyhenmeyer, G. A., Sherpa, P. Y., Weyer, N., Wouters, B., Yasunari, T., You, Q., and Zhang, Y.: High Mountain Areas, in: The Ocean and Cryosphere in a Changing Climate: Special Report of the Intergovernmental Panel on Climate Change, edited by Pörtner, H.-O., Roberts, D., Masson-Delmotte, V., Zhai, P., Tignor, M., Poloczanska, E., Mintenbeck, K., Alegría, A., Nicolai, M., Okem, A., Petzold, J., Rama, B., and Weyer, N., p. 131–202, Cambridge University Press, Cambridge, UK and New York, NY, USA, https://doi.org/10.1017/9781009157964.004, 2019.

Hoelzle, M., Azisov, E., Barandun, M., Huss, M., Farinotti, D., Gafurov, A., Hagg, W., Kenzhebaev, R., Kronenberg, M., Machguth, H., Merkushkin, A., Moldobekov, B., Petrov, M., Saks, T., Salzmann, N., Schöne, T., Tarasov, Y., Usubaliev, R., Vorogushyn, S., Yakovlev,

https://doi.org/10.5194/egusphere-2025-3462
Preprint. Discussion started: 17 November 2025

A., and Zemp, M.: Re-establishing glacier monitoring in Kyrgyzstan and Uzbekistan, Central Asia, Geoscientific Instrumentation, Methods and Data Systems, 6, 397–418, https://doi.org/10.5194/gi-6-397-2017, 2017.

Houska, T., Kraft, P., Chamorro-Chavez, A., and Breuer, L.: SPOTting Model Parameters Using a Ready-Made Python Package, PLOS ONE, 10, 1–22, https://doi.org/10.1371/journal.pone.0145180, 2015.

Houska, T., Kraft, P., Chamorro-Chavez, A., and Breuer, L.: SPOTPY: A Statistical Parameter Optimization Tool for Python, University of Giessen, Department of Geography, https://spotpy.readthedocs.io/en/latest/, accessed: 2024-05-20, 2023.

Hua, L., Zhao, T., and Zhong, L.: Future Changes in Drought over Central Asia under CMIP6 Forcing Scenarios, Journal of Hydrology: Regional Studies, 43, 101 191, https://doi.org/10.1016/j.ejrh.2022.101191, 2022.

Hugonnet, R., McNabb, R., Berthier, E., Menounos, B., Nuth, C., Girod, L., Farinotti, D., Huss, M., Dussaillant, I., Brun, F., and Kääb, A.: Accelerated global glacier mass loss in the early twenty-first century, Nature, 592, 726–731, https://doi.org/10.1038/s41586-021-03436-z, 2021.

Immerzeel, W. W., Lutz, A. F., Andrade, M., Bahl, A., Biemans, H., Bolch, T., Hyde, S., Brumby, S., Davies, B., Elmore, A., et al.: Importance and vulnerability of the world's water towers, Nature, 577, 364–369, 2020.

Jiang, F., Wen, S., Gao, M., and Zhu, A.: Assessment of NEX-GDDP-CMIP6 Downscale Data in Simulating Extreme Precipitation over the Huai River Basin, Atmosphere, 14, https://doi.org/10.3390/atmos14101497, 2023.

Jiang, J. and Zhou, T.: Agricultural Drought over Water-Scarce Central Asia Aggravated by Internal Climate Variability, Nature Geoscience, 16, 154–161, https://doi.org/10.1038/s41561-022-01111-0, 2023.

Kling, H., Fuchs, M., and Paulin, M.: Runoff conditions in the upper Danube basin under an ensemble of climate change scenarios, Journal of Hydrology, 424-425, 264–277, https://doi.org/https://doi.org/10.1016/j.jhydrol.2012.01.011, 2012.

Kochendorfer, J., Rasmussen, R., Wolff, M., Baker, B., Hall, M. E., Meyers, T., Landolt, S., Jachcik, A., Isaksen, K., Brækkan, R., and Leeper, R.: The quantification and correction of wind-induced precipitation measurement errors, Hydrology and Earth System Sciences, 21, 1973–1989, https://doi.org/10.5194/hess-21-1973-2017, 2017.

Kriegel, D., Mayer, C., Hagg, W., Vorogushyn, S., Duethmann, D., Gafurov, A., and Farinotti, D.: Changes in glacierisation, climate and runoff in the second half of the 20th century in the Naryn basin, Central Asia, Global and Planetary Change, 110, 51–61, 2013.

Lange, S.: Trend-preserving bias adjustment and statistical downscaling with ISIMIP3BASD (v1. 0), Geoscientific Model Development, 12, 3055–3070, 2019.

Lawrence, D., Hurtt, G., Arneth, A., Brovkin, V., Calvin, K., Jones, A. D., Jones, C., Lawrence, P., Noblet-Ducoudré, N., Pongratz, J., Seneviratne, S., and Shevliakova, E.: The Land Use Model Intercomparison Project (LUMIP) contribution to CMIP6: rationale and experimental design, Geoscientific Model Development, 9, 2973–2998, https://doi.org/10.5194/GMD-9-2973-2016, 2016.

Li, Z., Chen, Y., Li, Y., and Wang, Y.: Declining snowfall fraction in the alpine regions, Central Asia, Scientific Reports, 10, 3476, https://doi.org/10.1038/s41598-020-60303-z, 2020.

Liu, Y., Fang, Y., and Margulis, S. A.: High Mountain Asia UCLA Daily Snow Reanalysis, Version 1, https://doi.org/10.5067/HNAUGJQXSCVU, 2021a.

Liu, Y., Fang, Y., and Margulis, S. A.: Spatiotemporal distribution of seasonal snow water equivalent in High Mountain Asia from an 18-year Landsat–MODIS era snow reanalysis dataset, The Cryosphere, 15, 5261–5280, https://doi.org/10.5194/tc-15-5261-2021, 2021b.

Liu, Y., Fernández-Ortega, J., Mudarra, M., and Hartmann, A.: Pitfalls and a feasible solution for using KGE as an informal likelihood function in MCMC methods: DREAM$_{(ZS)}$ as an example, Hydrology and Earth System Sciences, 26, 5341–5355, https://doi.org/10.5194/hess-26-5341-2022, 2022.

https://doi.org/10.5194/egusphere-2025-3462
Preprint. Discussion started: 17 November 2025

Lutz, A., Immerzeel, W., Shrestha, A. B., and Bierkens, M.: Consistent increase in High Asia's runoff due to increasing glacier melt and precipitation, Nature Climate Change, 4, 587–592, 2014.

Ma, L., Hurtt, G., Chini, L., Sahajpal, R., Pongratz, J., Frolking, S., Stehfest, E., Goldewijk, K. K., O'leary, D., and Doelman, J.: Global rules for translating land-use change (LUH2) to land-cover change for CMIP6 using GLM2, Geoscientific Model Development, https://doi.org/10.5194/gmd-13-3203-2020, 2020.

Mantovan, P. and Todini, E.: Hydrological forecasting uncertainty assessment: Incoherence of the GLUE methodology, Journal of Hydrology, 330, 368–381, https://doi.org/10.1016/j.jhydrol.2006.04.046, hydro-ecological functioning of the Pang and Lambourn catchments, UK, 2006.

Mastrotheodoros, T., Pappas, C., Molnar, P., Burlando, P., Manoli, G., Parajka, J., Rigon, R., Széles, B., Bottazzi, M., Hadjidoukas, P., and Fatichi, S.: More green and less blue water in the Alps during warmer summers, Nature Climate Change, 10, 155–161, https://doi.org/10.1038/s41558-019-0676-5, 2020.

McKay, M. D., Beckman, R. J., and Conover, W. J.: A Comparison of Three Methods for Selecting Values of Input Variables in the Analysis of Output from a Computer Code, Technometrics, 21, 239–245, http://www.jstor.org/stable/1268522, 1979.

Miles, E. S., McCarthy, M., Dehecq, A., Kneib, M., Fugger, S., and Pellicciotti, F.: Health and Sustainability of Glaciers in High Mountain Asia, Nature Communications, https://doi.org/10.1038/s41467-021-23073-4, 2021.

Milner, A. M., Brown, L. E., and Hannah, D. M.: Hydroecological response of river systems to shrinking glaciers, Hydrological Processes, 23, 62–77, https://doi.org/10.1002/hyp.7197, 2009.

Muñoz Sabater, J., Dutra, E., Agustí-Panareda, A., Albergel, C., Arduini, G., Balsamo, G., Boussetta, S., Choulga, M., Harrigan, S., Hersbach, H., Martens, B., Miralles, D. G., Piles, M., Rodríguez-Fernández, N. J., Zsoter, E., Buontempo, C., and Thépaut, J.-N.: ERA5-Land: a state-of-the-art global reanalysis dataset for land applications, Earth System Science Data, 13, 4349–4383, https://doi.org/10.5194/essd-13-4349-2021, 2021.

Nemri, S. and Kinnard, C.: Comparing calibration strategies of a conceptual snow hydrology model and their impact on model performance and parameter identifiability, Journal of Hydrology, 582, 124 474, https://doi.org/10.1016/j.jhydrol.2019.124474, 2020.

Oudin, L., Hervieu, F., Michel, C., Perrin, C., Andréassian, V., Anctil, F., and Loumagne, C.: Which potential evapotranspiration input for a lumped rainfall–runoff model?: Part 2—Towards a simple and efficient potential evapotranspiration model for rainfall–runoff modelling, Journal of Hydrology, 303, 290–306, https://doi.org/https://doi.org/10.1016/j.jhydrol.2004.08.026, 2005.

Penna, D., Engel, M., Mao, L., Dell'Agnese, A., Bertoldi, G., and Comiti, F.: Tracer-based analysis of spatial and temporal variations of water sources in a glacierized catchment, Hydrology and Earth System Sciences, 18, 5271–5288, https://doi.org/10.5194/HESS-18-5271-2014, 2014.

Peña-Ramos, J. A., Bagus, P., and Fursova, D.: Water Conflicts in Central Asia: Some Recommendations on the Non-Conflictual Use of Water, Sustainability, 13, https://doi.org/10.3390/su13063479, 2021.

Pohl, E., Gloaguen, R., Andermann, C., and Knoche, M.: Glacier melt buffers river runoff in the Pamir Mountains, Water Resources Research, 53, 2467–2489, 2017.

Pritchard, H. D.: Asia's shrinking glaciers protect large populations from drought stress, Nature, 569, 649–654, 2019.

RGI Consortium: Randolph Glacier Inventory - A Dataset of Global Glacier Outlines, Version 6, Boulder, Colorado USA. NSIDC: National Snow and Ice Data Center, https://doi.org/https://doi.org/10.7265/4m1f-gd79, 2017.

https://doi.org/10.5194/egusphere-2025-3462
Preprint. Discussion started: 17 November 2025

Savéan, M., Delclaux, F., Chevallier, P., Wagnon, P., Gonga-Saholiariliva, N., Sharma, R., Neppel, L., and Arnaud, Y.: Water budget on the Dudh Koshi River (Nepal): Uncertainties on precipitation, Journal of Hydrology, 531, 850–862, https://doi.org/10.1016/j.jhydrol.2015.10.040, 2015.

Schaffhauser, T., Lange, S., Tuo, Y., and Disse, M.: Shifted discharge and drier soils: Hydrological projections for a Central Asian catchment, Journal of Hydrology: Regional Studies, 46, 101 338, https://doi.org/https://doi.org/10.1016/j.ejrh.2023.101338, 2023.

Schuster, P., Georgi, A., and Janzen, M.: MATILDA-Online: Cloud-based Workflow for Modeling wATer resources In gLacierizeD cAtchments, https://doi.org/10.5281/zenodo.15712744, 2025a.

Schuster, P., Georgi, A., and Tappe, A.-L.: MATILDA: Modeling wATer resources In gLacierizeD cAtchments, https://doi.org/10.5281/zenodo.14267360, 2025b.

Schuster, P., Tappe, A.-L., Georgi, A., Schneider, C., and Sauter, T.: MATILDA: A Cloud-based Open-Source Workflow for Modeling Water Resources in Glacierized Catchments, Geoscientific Model Development, manuscript submitted for publication, 2025c.

Shannon, S., Payne, A., Freer, J., Coxon, G., Kauzlaric, M., Kriegel, D., and Harrison, S.: A snow and glacier hydrological model for large catchments – case study for the Naryn River, central Asia, Hydrology and Earth System Sciences, 27, 453–480, https://doi.org/10.5194/hess-27-453-2023, 2023.

Shea, J. M., Menounos, B., Moore, R. D., and Tennant, C.: An approach to derive regional snow lines and glacier mass change from MODIS imagery, western North America, The Cryosphere, 7, 667–680, https://doi.org/10.5194/tc-7-667-2013, 2013.

Shean, D. E., Bhushan, S., Montesano, P., Rounce, D. R., Arendt, A., and Osmanoglu, B.: A Systematic, Regional Assessment of High Mountain Asia Glacier Mass Balance, Frontiers in Earth Science, 7, https://doi.org/10.3389/feart.2019.00363, 2020.

Siegfried, T., Mujahid, A. U. H., Marti, B., Molnar, P., Karger, D. N., and Yakovlev, A.: Unveiling the Future Water Pulse of Central Asia: A Comprehensive 21st Century Hydrological Forecast from Stochastic Water Balance Modeling, Climatic Change, 177, 141, https://doi.org/10.1007/s10584-024-03799-y, 2024.

Simons, G., Koster, R., and Droogers, P.: HiHydroSoil v2.0 - High Resolution Soil Maps of Global Hydraulic Properties, https://www.futurewater.nl/wp-content/uploads/2020/10/HiHydroSoil-v2.0-High-Resolution-Soil-Maps-of-Global-Hydraulic-Properties.pdf, 2020.

Sorg, A., Bolch, T., Stoffel, M., Solomina, O., and Beniston, M.: Climate change impacts on glaciers and runoff in Tien Shan (Central Asia), Nature Climate Change, 2, 725–731, 2012.

Stedinger, J. R., Vogel, R. M., Lee, S. U., and Batchelder, R.: Appraisal of the generalized likelihood uncertainty estimation (GLUE) method, Water Resources Research, 44, https://doi.org/10.1029/2008WR006822, 2008.

ter Braak, C. J. F. and Vrugt, J. A.: Differential Evolution Markov Chain with snooker updater and fewer chains, Statistics and Computing, 18, 435–446, https://doi.org/10.1007/s11222-008-9104-9, 2008.

Thrasher, B., Wang, W., Michaelis, A., Melton, F., Lee, T., and Nemani, R.: NASA Global Daily Downscaled Projections, CMIP6, Scientific Data, 9, https://doi.org/10.1038/s41597-022-01393-4, 2022.

Turner, B. M., Sederberg, P., Brown, S. D., and Steyvers, M.: A method for efficiently sampling from distributions with correlated dimensions, Psychological Methods, 18, 368–384, https://doi.org/10.1037/a0032222, 2013.

van Tiel, M., Stahl, K., Freudiger, D., and Seibert, J.: Glacio-Hydrological Model Calibration and Evaluation, WIREs Water, 7, e1483, https://doi.org/10.1002/wat2.1483, 2020.

Van Tiel, M., Van Loon, A. F., Seibert, J., and Stahl, K.: Hydrological Response to Warm and Dry Weather: Do Glaciers Compensate?, Hydrology and Earth System Sciences, 25, 3245–3265, https://doi.org/10.5194/hess-25-3245-2021, 2021.

https://doi.org/10.5194/egusphere-2025-3462
Preprint. Discussion started: 17 November 2025

Viviroli, D., Kummu, M., Meybeck, M., Kallio, M., and Wada, Y.: Increasing dependence of lowland populations on mountain water resources, Nature Sustainability, 3, 917–928, 2020.

Voldoire, A., Saint-Martin, D., Sénési, S., Decharme, B., Alias, A., Chevallier, M., Colin, J., Guérémy, J.-F., Michou, M., Moine, M.-P., Nabat, P., Roehrig, R., Salas y Mélia, D., Séférian, R., Valcke, S., Beau, I., Belamari, S., Berthet, S., Cassou, C., Cattiaux, J., Deshayes, J., Douville, H., Ethé, C., Franchistéguy, L., Geoffroy, O., Lévy, C., Madec, G., Meurdesoif, Y., Msadek, R., Ribes, A., Sanchez-Gomez, E., Terray, L., and Waldman, R.: Evaluation of CMIP6 DECK Experiments With CNRM-CM6-1, Journal of Advances in Modeling Earth Systems, 11, 2177–2213, https://doi.org/10.1029/2019MS001683, 2019.

Warszawski, L., Frieler, K., Huber, V., Piontek, F., Serdeczny, O., and Schewe, J.: The Inter-Sectoral Impact Model Intercomparison Project (ISI–MIP): Project framework, Proceedings of the National Academy of Sciences, 111, 3228–3232, https://doi.org/10.1073/pnas.1312330110, 2014.

WGMS: Fluctuations of Glaciers Database, World Glacier Monitoring Service (WGMS), Zurich, Switzerland, https://doi.org/10.5904/wgms-fog-2022-09, open access under requirement of correct citation, 2022.

Woo, M. and Thorne, R.: Snowmelt contribution to discharge from a large mountainous catchment in subarctic Canada, Hydrological Processes, 20, https://doi.org/10.1002/HYP.6205, 2006.

Wu, F., Jiao, D., Yang, X., Cui, Z., Zhang, H., and Wang, Y.: Evaluation of NEX-GDDP-CMIP6 in simulation performance and drought capture utility over China – based on DISO, Hydrology Research, https://doi.org/10.2166/nh.2023.140, 2023a.

Wu, X., Su, J., Ren, W., Lü, H., and Yuan, F.: Statistical comparison and hydrological utility evaluation of ERA5-Land and IMERG precipitation products on the Tibetan Plateau, Journal of Hydrology, 620, 129 384, https://doi.org/https://doi.org/10.1016/j.jhydrol.2023.129384, 2023b.

Wu, X., Tang, W., Chen, F., Wang, S., Bakhtiyorov, Z., Liu, Y., and Guan, Y.: Attribution and Risk Projections of Hydrological Drought Over Water-Scarce Central Asia, Earth's Future, 13, e2024EF005 243, https://doi.org/10.1029/2024EF005243, 2025.

Xenarios, S., Gafurov, A., Schmidt-Vogt, D., Sehring, J., Manandhar, S., Hergarten, C., Shigaeva, J., and Foggin, M.: Climate change and adaptation of mountain societies in Central Asia: uncertainties, knowledge gaps, and data constraints, Regional Environmental Change, 19, 1339–1352, 2019.

Yamazaki, D., Ikeshima, D., Tawatari, R., Yamaguchi, T., O'Loughlin, F., Neal, J. C., Sampson, C. C., Kanae, S., and Bates, P. D.: A high-accuracy map of global terrain elevations, Geophysical Research Letters, 44, 5844–5853, https://doi.org/https://doi.org/10.1002/2017GL072874, 2017.

Yang, L.-s., Feng, Q., Adamowski, J., Alizadeh, M., Yin, Z., Wen, X., and Zhu, M.: The role of climate change and vegetation greening on the variation of terrestrial evapotranspiration in northwest China's Qilian Mountains, The Science of the Total Environment, p. 143532, https://doi.org/10.1016/j.scitotenv.2020.143532, 2020.

Yang, T., Li, Q., Ahmad, S., Zhou, H., and Li, L.: Changes in Snow Phenology from 1979 to 2016 over the Tianshan Mountains, Central Asia, Remote Sensing, 11, 499, https://doi.org/10.3390/rs11050499, 2019.

Yuan, H.-H., Huang, J.-B., Ning, L.-K., Catu, F., Zhou, J.-W., Qiao, C., Yin, M., and Luo, Y.: Evaluation of precipitation extremes over the Tibetan plateau using the NASA global daily downscaled datasets NEX-GDDP-CMIP6, Advances in Climate Change Research, 14, 884–895, https://doi.org/https://doi.org/10.1016/j.accre.2023.12.001, 2023.

Zhang, Y., Yan, Z., Song, J., Wei, A., Sun, H., and Cheng, D.: Analysis for spatial-temporal matching pattern between water and land resources in Central Asia, Hydrology Research, 51, 994–1008, https://doi.org/10.2166/nh.2020.177, 2020.

https://doi.org/10.5194/egusphere-2025-3462
Preprint. Discussion started: 17 November 2025

Zhao, P. and He, Z.: A First Evaluation of ERA5-Land Reanalysis Temperature Product Over the Chinese Qilian Mountains, Frontiers in Earth Science, 10, https://doi.org/10.3389/feart.2022.907730, 2022.

Zou, W., Cao, S., and Tan, W.: Evaluating NEX-GDDP-CMIP6 Performance in Complex Terrain for Forecasting Key Freezing Rain Factors, Theoretical and Applied Climatology, 155, 9289–9304, https://doi.org/10.1007/s00704-024-05159-3, 2024.

https://doi.org/10.5194/egusphere-2025-3462
Preprint. Discussion started: 17 November 2025

Table 1. Characteristics of the example site "Kyzylsuu" as calculated by the MATILDA catchment routine.

Catchment Area [km^2]	295.68
Glacierized Area [km^2]	31.83
Glacierized Fraction [%]	10.8
Mean Catchment Elevation [m.a.s.l.]	3294
Catchment Elevation Range [m.a.s.l.]	3284 to 4771
ERA5-Land Reference Elevation [m.a.s.l.]	3337
Mean Glacier Elevation [m.a.s.l.]	4002
Latitude of Catchment Center [°]	42.18
No. of Glaciers (RGI 6.0)	38

https://doi.org/10.5194/egusphere-2025-3462
Preprint. Discussion started: 17 November 2025

Table 2. Calibration workflow, including methods, criteria, and sample sizes for each calibration step, and final parameter values.

	Step 1 "Input correction"	**Step 2 "Snow"**	**Step 3 "Glaciers"**	**Step 4 "Soil & Routing"**	**Final**
Method:	LHS	LHS	LHS (1-D)	DEMCz	
Sampling Criteria	k = 3, p = 8	k = 5, p = 3	-	M = 4, N_{burn} = 500, $\hat{R}$ = 0.8	
Sample size:	279'936	14'400	5'000	85'400	
Filter Criteria:	$\text{MAE}_{smb} < 100$ mm $\text{KGE}_{swe} > 0.7$ KGE_{r} (best 10%)	$\text{KGE}_{swe} > 0.8$	$\text{MAE}_{smb} < 100$ mm	$\text{MAE}_{smb} < 100$ mm $\text{KGE}_{r} > 0.88$ $\text{KGE}_{r,s} > 0.88$ $\text{KGE}_{r,w} > 0.24$	
SFCF	*1*				1
CET	*0*				0
PCORR	**0.58** ± **0.03**	*0.58*			0.58
lr_{temp}	**-0.006** ± 0.003	*-6×10^{-3}*			-6×10^{-3}
lr_{prec}	(**1.5**±0.5)×**10**$^{-3}$	*1.5×10^{-3}*			1.5×10^{-3}
CFR	**0.15***	*0.15**			0.15
TT_{snow}	-1.00 ± 0.45	**-1.45** ± 0.05	*-1.45*		-1.45
TT_{diff}	1.23 ± 0.55	**0.76** ± 0.17	*0.76*		0.76
$\text{CFMAX}_{\text{snow}}$	3.29 ± 0.48	**3.37** ± 0.42	*3.37*		3.37
$\text{CFMAX}_{\text{rel}}$	1.54 ± 0.22	*2.0**	**[1.2, 1.53]**	**1.256**	1.26
CWH	*0.1**	*0.1**	*0.1**	**1.17×10**$^{-4}$	1.17×10^{-4}
AG	*0.055**	*0.055**	*0.055**	**0.549**	0.55
BETA	1.78 ± 0.7	*1.0**	*1.0**	**1.0**	1.0
FC	*250**	*250**	*250**	**99.160**	99.16
LP	*0.7**	*0.7**	*0.7**	**0.998**	1.0
K0	*0.055**	*0.055**	*0.055**	**0.010**	0.01
K1	*0.055**	*0.055**	*0.055**	**0.010**	0.01
K2	*0.04**	*0.04**	*0.04**	**0.150**	0.15
PERC	*1.5**	*1.5**	*1.5**	**0.092**	0.09
UZL	*120**	*120**	*120**	**126.412**	126.41
MAXBAS	*3.0**	*3.0**	*3.0**	**2.0**	2.0

Legend: **Calibration parameter** – *Fixed parameter (* default)*

k = number of divisions, p = number of parameters,

M = number of MCMC chains, N_{burn} = burn-in samples,

$\hat{R}$ = Gelman–Rubin convergence statistic

https://doi.org/10.5194/egusphere-2025-3462
Preprint. Discussion started: 17 November 2025

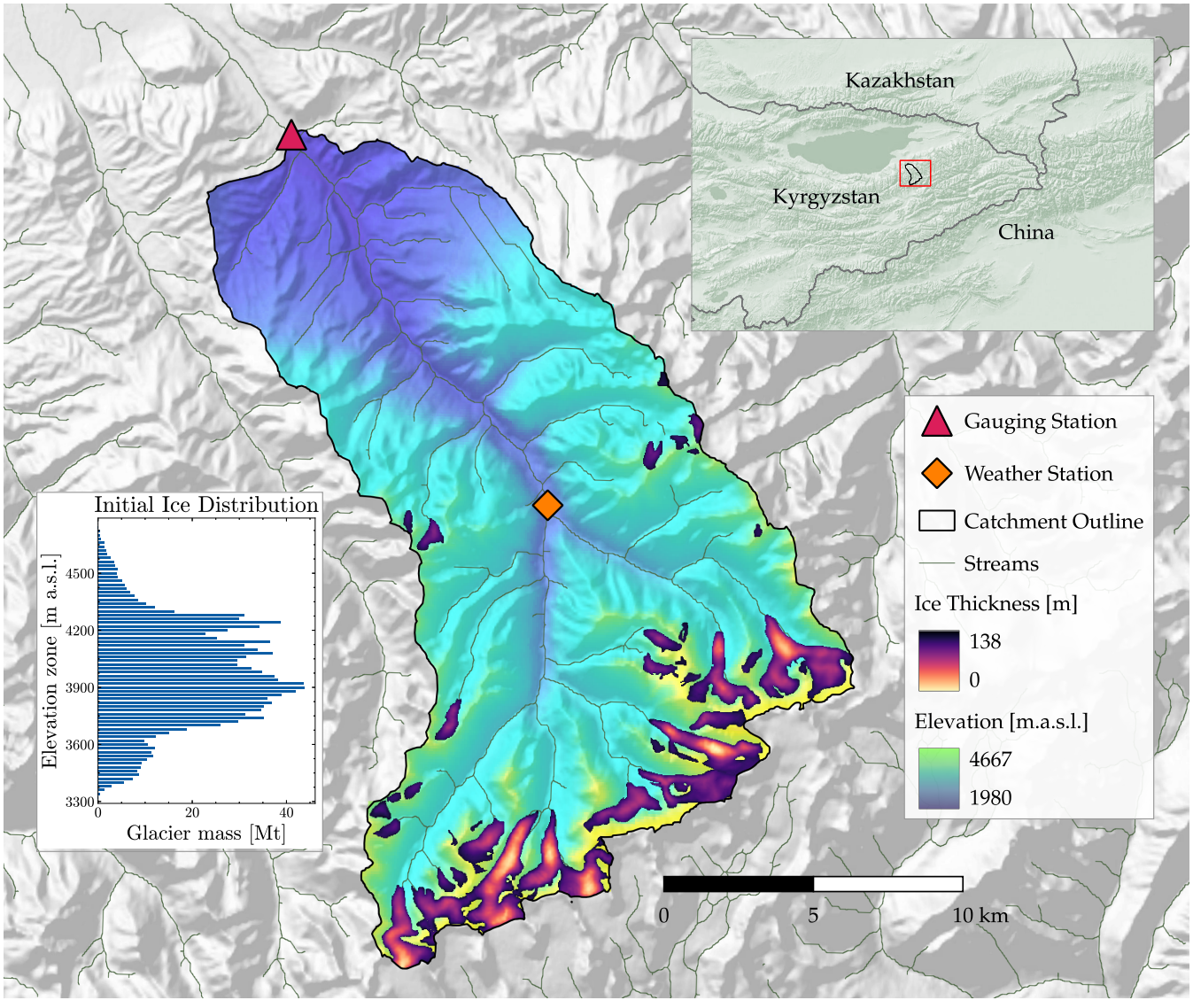

Figure 1. Overview of the Kyzylsuu catchment in the northern Tian Shan, Kyrgyzstan. Color gradients show elevation (MERIT DEM, Yamazaki et al. 2017) and glacier ice thickness according to the consensus estimate by Farinotti et al. (2019). Markings locate the weather (square) and discharge stations (triangle) used in this study. The barplot depicts the initial glacier ice distribution by elevation band in 2000.

https://doi.org/10.5194/egusphere-2025-3462
Preprint. Discussion started: 17 November 2025

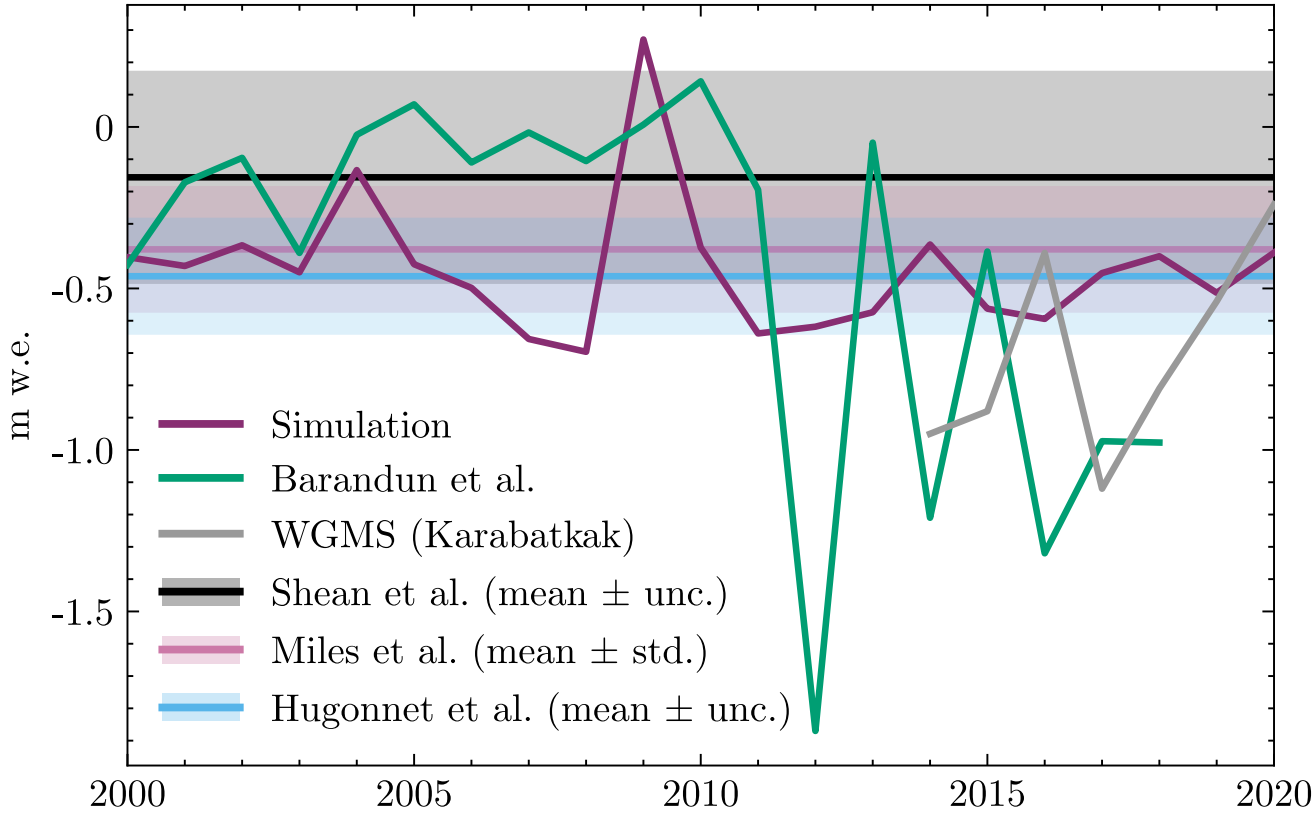

Figure 2. Surface mass balance (SMB) estimates for glaciers in the Kyzylsuu catchment. Annually resolved values shown for the MATILDA simulation results, in-situ observations of Kara-Batkak glacier (WGMS, 2022), and a multi-method approach for the seven largest glaciers Barandun et al. (2021). Multi-annual averages of geodetic estimates shown as horizontal lines with uncertainty range as shaded bands for the seven largest glaciers (Miles et al., 2021) and all 38 glaciers (Shean et al., 2020; Hugonnet et al., 2021), respectively.

https://doi.org/10.5194/egusphere-2025-3462
Preprint. Discussion started: 17 November 2025

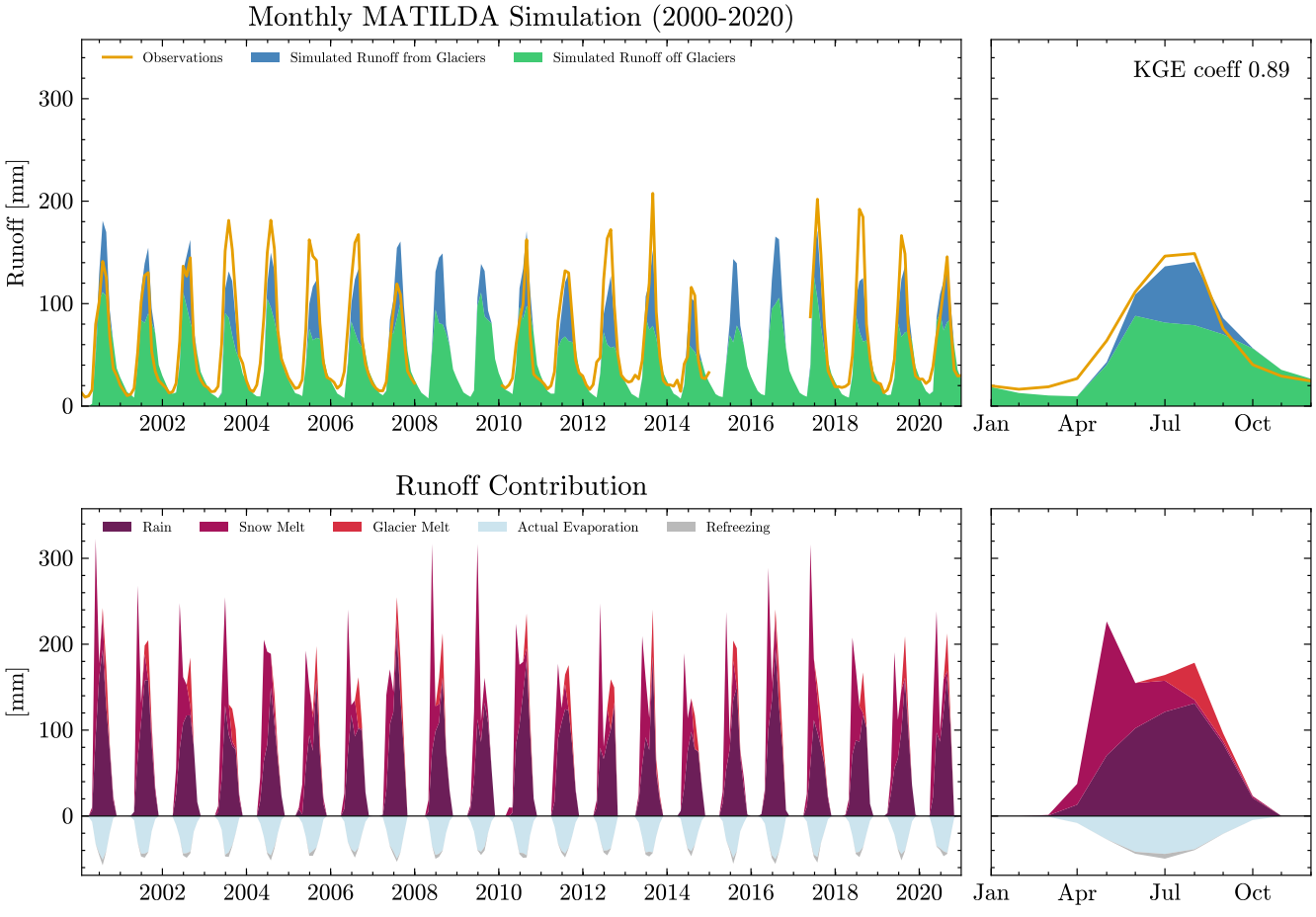

Figure 3. Monthly MATILDA simulations for the Kyzylsuu catchment (2000–2020). Observed and simulated discharge (top), and positive and negative modeled runoff contributions (bottom) shown as time series (left) and average annual cycles (right).

https://doi.org/10.5194/egusphere-2025-3462
Preprint. Discussion started: 17 November 2025

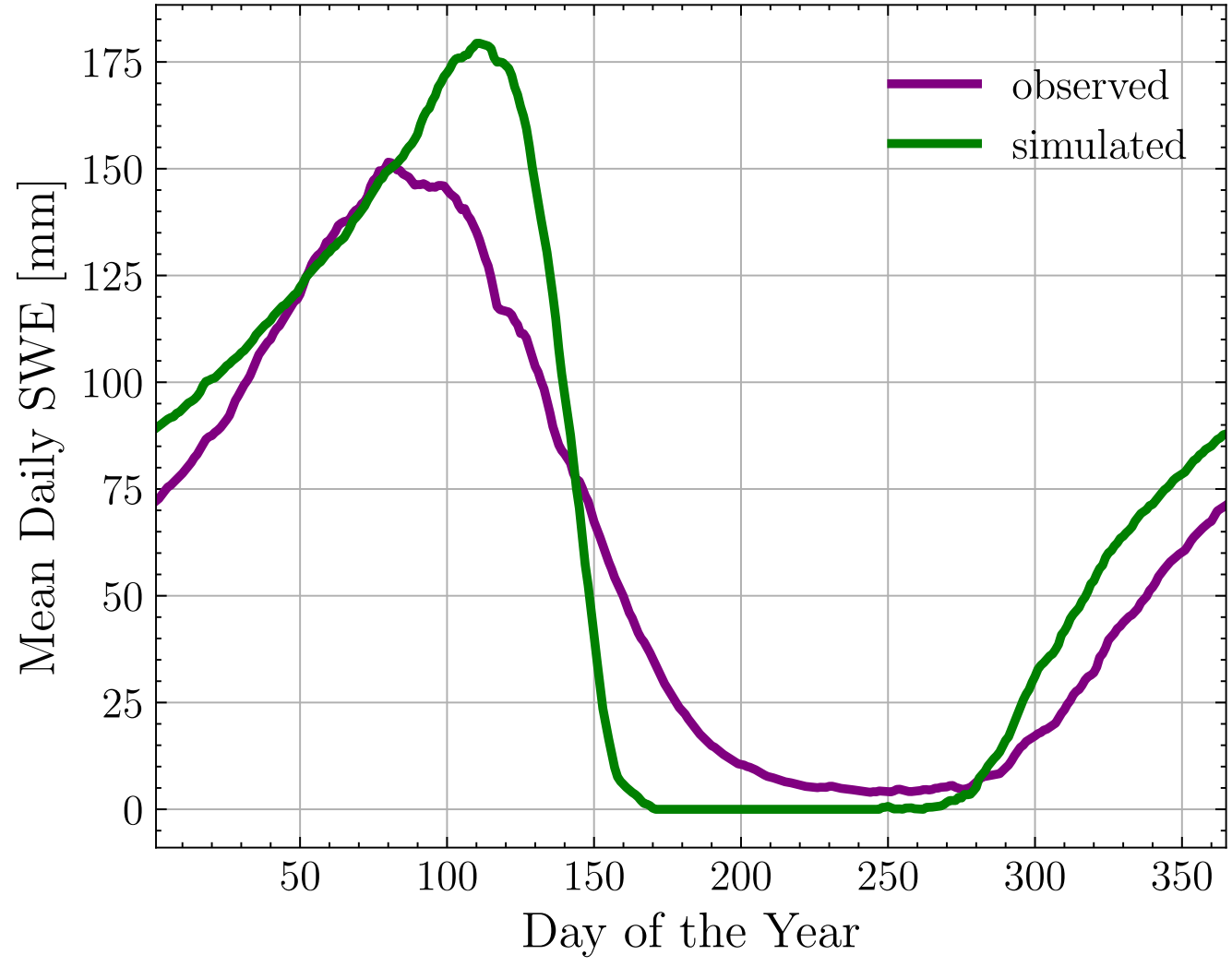

Figure 4. Mean annual cycle of daily snow water equivalent (SWE) in the non-glacierized part of the Kyzylsuu catchment during 2000–2017. Simulated SWE is compared to the ensemble mean of the High Mountain Asia Daily Snow Reanalysis (Liu et al., 2021a).

https://doi.org/10.5194/egusphere-2025-3462
Preprint. Discussion started: 17 November 2025

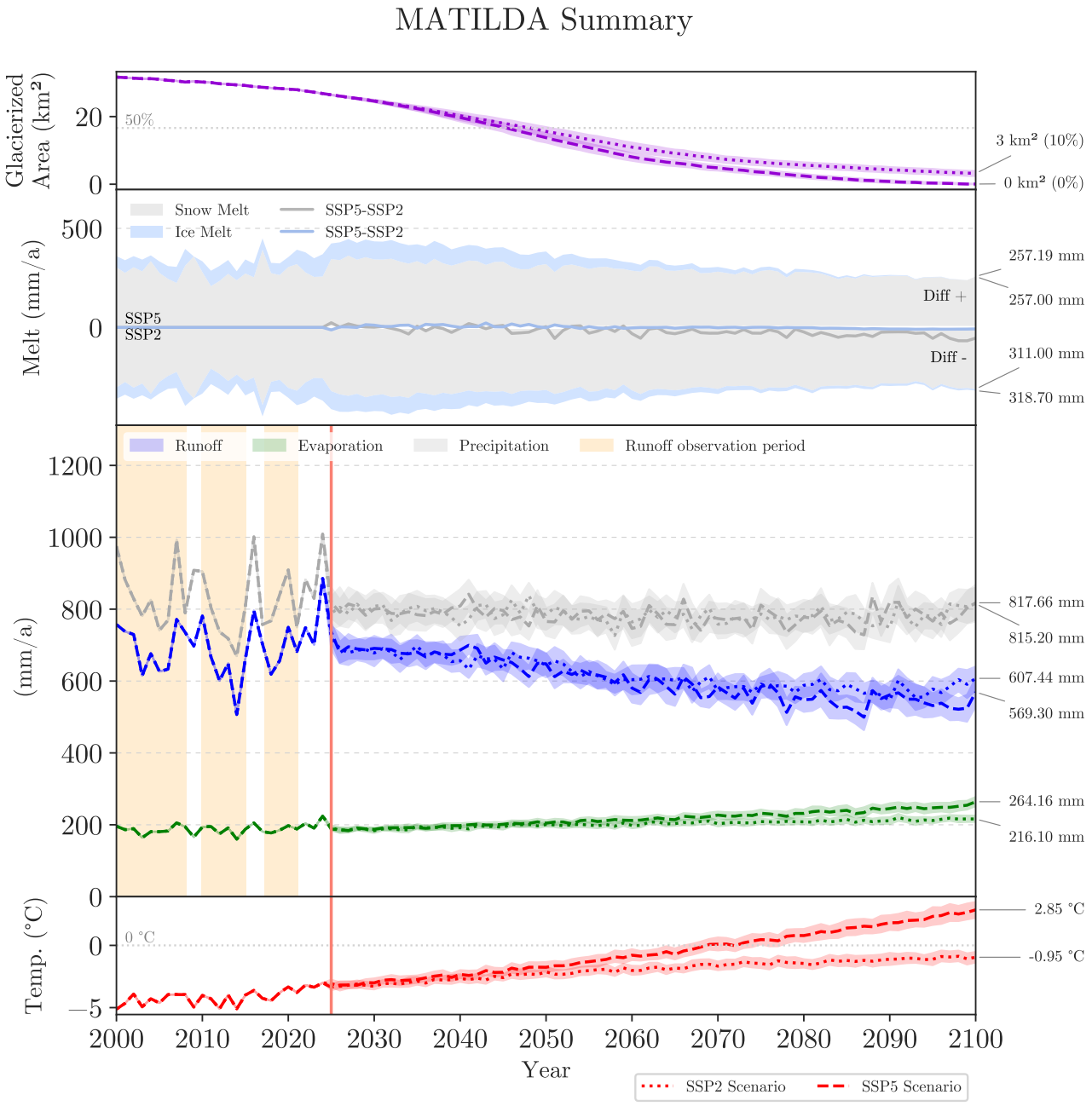

Figure 5. Summary of key hydrological and climatic variables for the Kyzylsuu catchment under SSP2 and SSP5 scenarios from 2000 to 2100. Panels show (top to bottom): glacierized area evolution; annual snow and ice melt; total runoff, precipitation, and actual evapotranspiration; and mean annual air temperature. In the melt panel, shadings indicate runoff contributions while solid lines show differences between the scenarios. In all other panels, lines represent ensemble means, with shaded areas indicating the 90% confidence interval of the ensemble. Vertical orange shading shows observed runoff periods. The vertical red line separates calibration and projection periods.

https://doi.org/10.5194/egusphere-2025-3462
Preprint. Discussion started: 17 November 2025

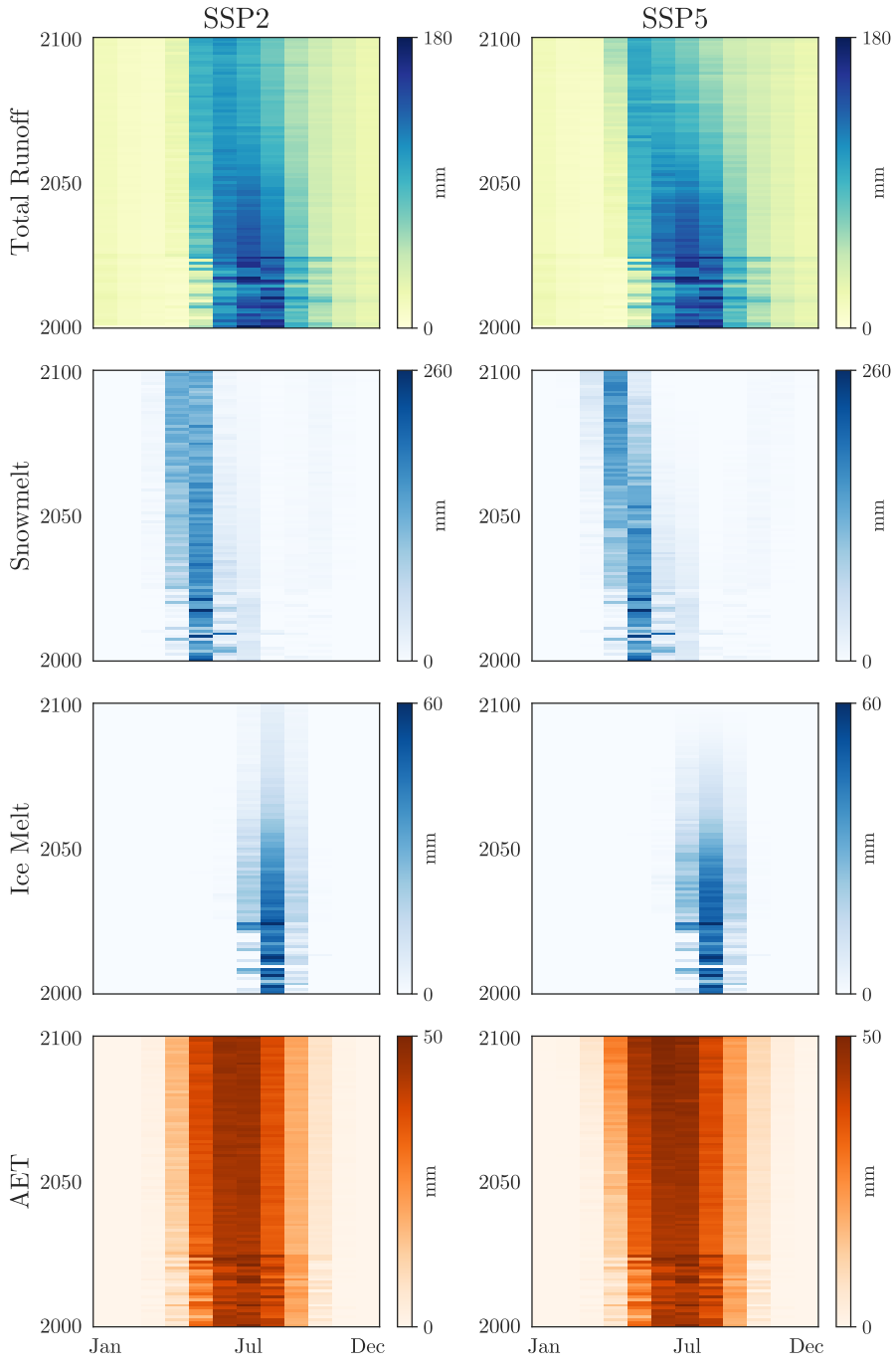

Figure 6. Annual cycles of runoff, snowmelt, ice melt, and actual evapotranspiration from 2000 to 2100 under SSP2 and SSP5 scenarios. Each panel shows monthly sums (x-axis: months; y-axis: years), highlighting seasonal patterns and long-term trends.

https://doi.org/10.5194/egusphere-2025-3462
Preprint. Discussion started: 17 November 2025

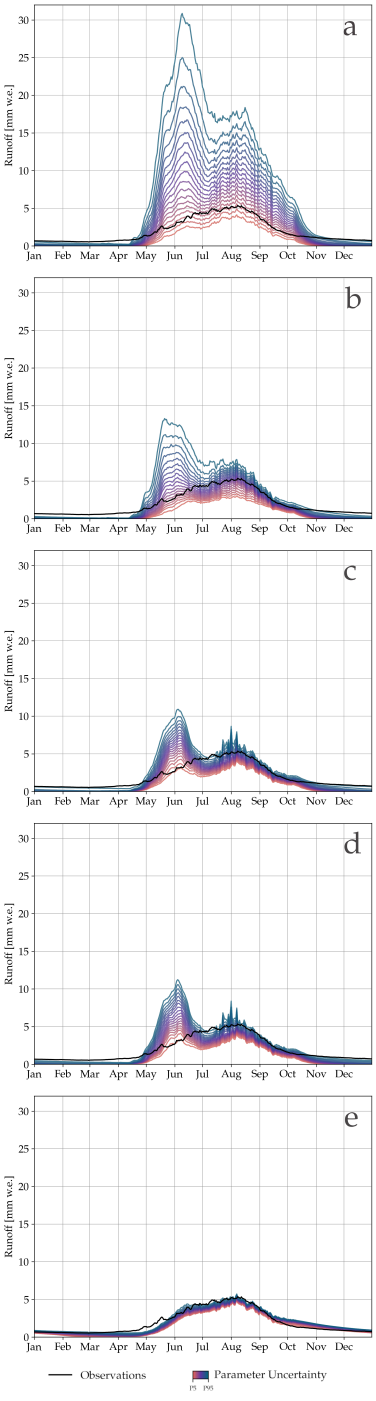

Figure 7. Average annual cycle of the simulated total runoff parameter uncertainty. Colored lines show percentiles (5 % to 95 %) of 20'000 random samples of simulated runoff in the calibration period (2000–2017) compared to observations. Subfigures represent different calibration steps: **(a)** no constraints, 21 open parameters; **(b)** external parameters fixed, 18 open parameters; **(c)** snow routine calibrated, 12 open parameters; **(d)** glacier routine calibrated, 11 open parameters, ice melt rate constrained; **(e)** all runs of (d) with $\mathrm{KGE}_r > 0.8$.

https://doi.org/10.5194/egusphere-2025-3462
Preprint. Discussion started: 17 November 2025

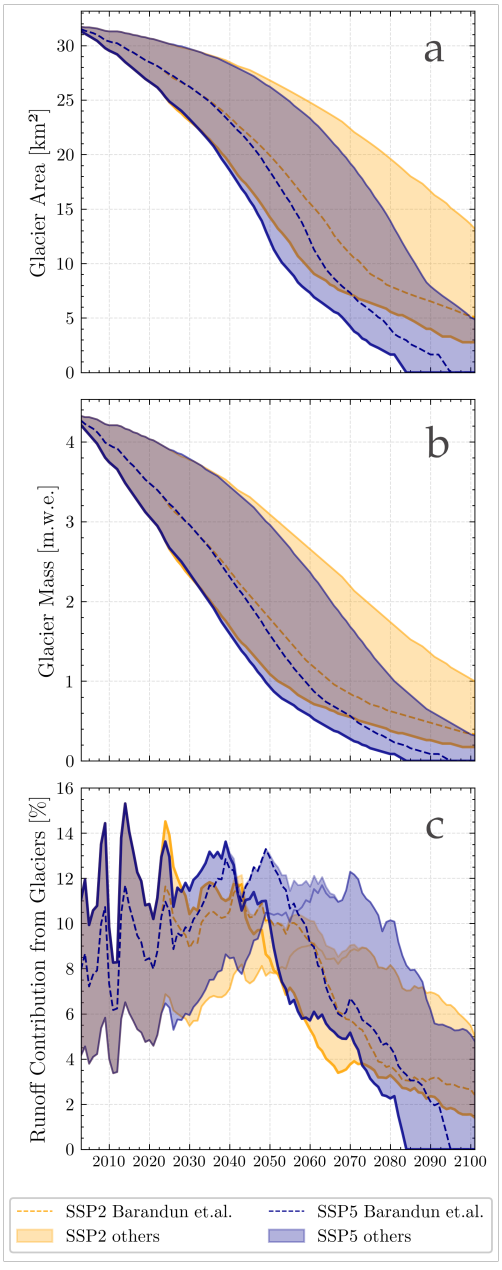

Figure 8. Uncertainty in glacier projections due to inconsistency in calibration data. Lines represent runs of the calibrated model in two SSP scenarios with the range of ice melt rates supported by the literature: **bold lines** for the lower bound calibrated to the catchment mean SMB of Shean et al. (2020) (2.11 mm K^{-1} d^{-1}), **thin lines** for the upper bound calibrated on Karabatkak's SMB according to WGMS (2022) (6.11 mm K^{-1} d^{-1}), **dashed lines** for the calibrated best estimate based on Barandun et al. (2021) (4.2 mm K^{-1} d^{-1}), smoothed with a three-year moving average. The shading represents the range of predictions between the bounds in steps of 10 %. **(a)** Simulated total glacier area; **(b)** Simulated total glacier mass; **(c)** Simulated contribution of glacier melt to total catchment runoff.

https://doi.org/10.5194/egusphere-2025-3462
Preprint. Discussion started: 17 November 2025

Table A1. Datasets used in the present study.

Dataset	Source
Meteorological observations	Research Institute of Water Problems and Hydro-energy Problems of the Kyrgyz Republic Academy of Sciences (IWP); Institute of Ecology and Geography of the Chinese Academy of Science
Gauging station	Hydro-meteorological Service under the Ministry of Emergency Situation of the Kyrgyz Republic (Kyrgyz HydroMet)
Ice thickness	Farinotti, D., Huss, M., Fürst, J. J., Landmann, J., Machguth, H., Maussion, F., and Pandit, A.: A consensus estimate for the ice thickness distribution of all glaciers on Earth, Nature Geoscience, 12, 168–173, https://doi.org/10.1038/s41561-019-0300-3, 2019.
ERA5-Land	Muñoz Sabater, J., et al.: ERA5-Land: a state-of-the-art global reanalysis dataset for land applications, Earth System Science Data, 13, 4349–4383, https://doi.org/10.5194/essd-13-4349-2021, 2021. GEE: https://developers.google.com/earth-engine/datasets/catalog/ECMWF_ERA5_LAND_DAILY_AGGR
RGI 6.0	RGI Consortium: Randolph Glacier Inventory - A dataset of global glacier outlines, Version 6, Boulder, Colorado USA. NSIDC: https://doi.org/10.7265/4m1f-gd79, 2017.
MERIT-DEM	Yamazaki, D., et al.: A high-accuracy map of global terrain elevations, Geophysical Research Letters, 44, 5844–5853, https://doi.org/10.1002/2017GL072874, 2017. GEE: https://developers.google.com/earth-engine/datasets/catalog/MERIT_DEM_v1_0_3
SMB data – Shean et.al.	Shean, D. E., et al.: A systematic, regional assessment of High Mountain Asia glacier mass balance, Frontiers in Earth Science, 7, https://doi.org/10.3389/feart.2019.00363, 2020.
SMB data – Barandun et.al.	Barandun, M., et al.: Hot spots of glacier mass balance variability in Central Asia, Geophysical Research Letters, 48, https://doi.org/10.1029/2020GL092084, 2021.
SMB data – Miles et.al.	Miles, E. S., et al.: Health and sustainability of glaciers in High Mountain Asia, Nature Communications, https://doi.org/10.1038/s41467-021-23073-4, 2021.
SMB data – WGMS	WGMS: Fluctuations of Glaciers Database, Zurich, https://doi.org/10.5904/wgms-fog-2022-09, 2022.
NEX-GDDP-CMIP6	Thrasher, B., et al.: NASA Global Daily Downscaled Projections, CMIP6, Scientific Data, 9, https://doi.org/10.1038/s41597-022-01393-4, 2022. GEE: https://developers.google.com/earth-engine/datasets/catalog/NASA_GDDP-CMIP6
High Mountain Asia Daily Snow Reanalysis	Liu, Y., Fang, Y., and Margulis, S. A.: High Mountain Asia UCLA Daily Snow Reanalysis, Version 1, https://doi.org/10.5067/HNAUGJQXSCVU, 2021a.

https://doi.org/10.5194/egusphere-2025-3462
Preprint. Discussion started: 17 November 2025

Table A2. List of all CMIP6 models used as future climate forcing. This study used a downscaled version called NEX-GDDP-CMIP6 by Thrasher et al. (2022) which was accessed via Google Earth Engine (https://developers.google.com/earth-engine/datasets/catalog/NASA_GDDP-CMIP6) in two emission scenarios (SSP2 and SSP5).

Applied CMIP6 Models
ACCESS-CM2
ACCESS-ESM1-5
BCC-CSM2-MR
CESM2
CESM2-WACCM
CMCC-CM2-SR5
CMCC-ESM2
CNRM-CM6-1
CNRM-ESM2-1
CanESM5
EC-Earth3
EC-Earth3-Veg-LR
FGOALS-g3
GFDL-CM4_gr1
GFDL-CM4_gr2
GFDL-ESM4
GISS-E2-1-G
HadGEM3-GC31-LL
INM-CM4-8
INM-CM5-0
IPSL-CM6A-LR
KACE-1-0-G
KIOST-ESM
MIROC-ES2L
MIROC6
MPI-ESM1-2-HR
MPI-ESM1-2-LR
MRI-ESM2-0
NESM3
NorESM2-MM
UKESM1-0-LL

https://doi.org/10.5194/egusphere-2025-3462
Preprint. Discussion started: 17 November 2025

Table A3. Ensemble means and standard deviation for selected variables from 2000 to 2100 for SSP2. Values are given as decadal mean (± ensemble standard deviation). Temperatures are given in °C, all other values are given in mm w.e.

Variable	**2000–2010**	**2010–2020**	**2020–2030**	**2030–2040**	**2040–2050**	**2050–2060**	**2060–2070**	**2070–2080**	**2080–2090**	**2090–2100**
Mean Catchment Temperature	-3.7	-3.5	-2.6	-2.3	-1.9	-1.6	-1.4	-1.1	-0.9	-0.7
	(± 0.4)	(± 0.5)	(± 0.6)	(± 0.8)	(± 0.9)	(± 0.9)	(± 1.0)	(± 1.1)	(± 1.1)	(± 1.2)
Mean Temperature Glacierized Area	-8.1	-7.9	-7.1	-6.9	-6.7	-6.7	-6.8	-6.8	-6.8	-6.7
	(± 0.4)	(± 0.5)	(± 0.6)	(± 0.8)	(± 0.7)	(± 0.7)	(± 0.7)	(± 0.9)	(± 1.0)	(± 1.0)
Potential Evaporation	258.1	266.1	287.9	298.0	309.1	319.7	327.6	336.4	340.0	347.3
	(± 15.1)	(± 10.0)	(± 20.8)	(± 27.3)	(± 28.2)	(± 29.7)	(± 32.4)	(± 34.4)	(± 36.7)	(± 38.1)
Actual Evaporation	185.4	186.3	193.3	189.9	196.5	199.6	204.7	207.0	210.3	214.8
	(± 11.9)	(± 11.9)	(± 17.2)	(± 18.7)	(± 18.8)	(± 21.0)	(± 21.3)	(± 21.9)	(± 24.8)	(± 24.9)
Total Precipitation	854.5	810.7	834.1	791.4	794.1	775.9	778.0	773.1	774.1	787.8
	(± 80.4)	(± 92.9)	(± 115.7)	(± 115.7)	(± 122.0)	(± 116.8)	(± 114.9)	(± 117.1)	(± 119.1)	(± 114.1)
Total Melt	345.5	333.7	398.0	421.3	390.5	364.2	343.1	320.1	309.2	302.8
	(± 24.7)	(± 42.2)	(± 48.4)	(± 57.2)	(± 58.4)	(± 66.3)	(± 70.2)	(± 66.0)	(± 63.8)	(± 69.6)
Runoff Without Glaciers	548.4	515.4	545.4	520.2	530.2	527.7	538.2	539.4	545.9	555.5
	(± 52.6)	(± 71.6)	(± 84.6)	(± 94.8)	(± 99.7)	(± 97.6)	(± 97.4)	(± 93.8)	(± 94.9)	(± 97.0)
Runoff From Glaciers	157.1	156.4	173.5	154.4	126.7	93.2	61.7	42.0	31.0	23.4
	(± 26.2)	(± 14.7)	(± 32.2)	(± 27.9)	(± 25.7)	(± 28.5)	(± 24.4)	(± 16.5)	(± 13.5)	(± 13.4)
Total Runoff	705.5	671.8	718.9	674.6	656.9	620.9	599.9	581.4	576.9	579.0
	(± 57.2)	(± 80.1)	(± 94.2)	(± 90.9)	(± 91.2)	(± 93.3)	(± 92.6)	(± 90.3)	(± 93.5)	(± 96.1)
Snow Off Glaciers	227.7	219.0	257.6	290.5	284.3	284.8	290.6	286.4	282.2	284.8
	(± 33.0)	(± 31.3)	(± 53.9)	(± 57.5)	(± 53.7)	(± 54.8)	(± 63.0)	(± 62.2)	(± 57.7)	(± 61.7)
Snow On Glaciers	64.9	60.5	56.2	50.3	40.5	30.4	22.3	16.4	12.6	9.5
	(± 6.3)	(± 3.4)	(± 6.8)	(± 10.4)	(± 10.9)	(± 10.8)	(± 9.3)	(± 7.4)	(± 6.5)	(± 6.1)
Snow Melt Off Glaciers	231.7	215.0	258.7	290.6	283.4	284.9	291.0	284.8	283.4	283.2
	(± 34.4)	(± 42.3)	(± 49.6)	(± 59.0)	(± 54.8)	(± 57.6)	(± 64.6)	(± 61.3)	(± 59.0)	(± 65.0)
Total Melt On Glaciers	113.9	118.7	139.2	130.7	107.1	79.3	52.1	35.4	25.8	19.6
	(± 20.4)	(± 10.4)	(± 28.6)	(± 27.4)	(± 24.5)	(± 25.4)	(± 21.4)	(± 14.4)	(± 11.6)	(± 11.4)
Glacier Melt	55.3	61.9	84.7	82.0	67.7	49.6	30.3	19.4	13.6	10.4
	(± 22.3)	(± 10.7)	(± 32.7)	(± 32.2)	(± 23.8)	(± 20.0)	(± 16.3)	(± 10.9)	(± 7.6)	(± 7.0)
Snow Melt On Glaciers	58.6	56.8	54.6	48.7	39.4	29.7	21.8	15.9	12.3	9.2
	(± 4.4)	(± 4.3)	(± 6.7)	(± 9.7)	(± 10.7)	(± 10.5)	(± 9.1)	(± 7.1)	(± 6.4)	(± 5.9)

https://doi.org/10.5194/egusphere-2025-3462
Preprint. Discussion started: 17 November 2025

Table A4. Ensemble means and standard deviation for selected variables from 2000 to 2100 for SSP5. Values are given as decadal mean (± ensemble standard deviation). Temperatures are given in °C, all other values are given in mm w.e.

Variable	**2000–2010**	**2010–2020**	**2020–2030**	**2030–2040**	**2040–2050**	**2050–2060**	**2060–2070**	**2070–2080**	**2080–2090**	**2090–2100**
Mean Catchment Temperature	-3.7	-3.5	-2.7	-2.3	-1.8	-1.0	0.0	1.0	2.2	3.6
	(± 0.5)	(± 0.5)	(± 0.6)	(± 0.6)	(± 0.5)	(± 0.6)	(± 0.7)	(± 0.6)	(± 0.7)	(± 1.0)
Mean Temperature Glacierized Area	-8.1	-7.9	-7.1	-6.8	-6.4	-5.9	-5.6	-4.9	-4.2	-2.8
	(± 0.5)	(± 0.5)	(± 0.6)	(± 0.6)	(± 0.4)	(± 0.5)	(± 0.6)	(± 0.6)	(± 0.7)	(± 1.0)
Potential Evaporation	258.1	266.1	282.3	290.9	309.4	333.4	368.5	394.6	434.6	482.0
	(± 15.8)	(± 10.5)	(± 19.5)	(± 15.8)	(± 18.6)	(± 14.9)	(± 22.2)	(± 22.0)	(± 22.5)	(± 29.6)
Actual Evaporation	185.4	186.3	182.4	184.7	191.9	204.2	211.9	220.5	223.8	236.8
	(± 12.5)	(± 12.5)	(± 13.9)	(± 12.9)	(± 11.6)	(± 17.3)	(± 20.6)	(± 23.3)	(± 26.5)	(± 30.2)
Total Precipitation	854.5	810.7	803.3	833.8	784.2	798.5	746.5	833.2	768.1	781.7
	(± 84.2)	(± 97.3)	(± 75.2)	(± 132.2)	(± 96.4)	(± 113.0)	(± 135.3)	(± 135.2)	(± 122.8)	(± 125.0)
Total Melt	345.5	333.7	419.4	432.1	421.1	388.2	311.3	315.1	242.2	235.9
	(± 25.9)	(± 44.1)	(± 55.3)	(± 55.1)	(± 62.9)	(± 67.0)	(± 66.2)	(± 64.3)	(± 59.6)	(± 56.1)
Runoff Without Glaciers	548.4	515.4	525.3	563.9	530.6	554.0	515.4	593.3	546.0	538.8
	(± 55.0)	(± 75.0)	(± 61.5)	(± 74.8)	(± 86.9)	(± 99.2)	(± 98.8)	(± 108.9)	(± 105.8)	(± 99.7)
Runoff From Glaciers	157.1	156.4	158.7	148.8	139.9	108.7	65.0	38.0	12.8	0.0
	(± 27.5)	(± 15.4)	(± 22.3)	(± 17.9)	(± 18.1)	(± 17.5)	(± 11.9)	(± 8.6)	(± 10.4)	(± 0.0)
Total Runoff	705.5	671.8	684.0	712.6	670.5	662.6	580.5	631.4	558.8	538.8
	(± 59.9)	(± 83.8)	(± 59.0)	(± 75.9)	(± 76.5)	(± 92.6)	(± 96.9)	(± 106.1)	(± 109.1)	(± 99.7)
Snow Off Glaciers	227.7	219.0	287.1	304.5	292.9	291.5	250.4	283.0	227.3	238.7
	(± 34.5)	(± 32.8)	(± 37.3)	(± 63.5)	(± 60.7)	(± 61.6)	(± 64.3)	(± 56.3)	(± 52.0)	(± 51.5)
Snow On Glaciers	64.9	60.5	62.1	56.6	43.0	30.1	16.4	9.5	2.7	0.0
	(± 6.6)	(± 3.6)	(± 6.5)	(± 11.8)	(± 8.0)	(± 5.7)	(± 5.0)	(± 2.5)	(± 2.4)	(± 0.0)
Snow Melt Off Glaciers	231.6	214.9	286.0	304.2	298.6	293.3	253.9	281.0	230.5	235.9
	(± 36.0)	(± 44.3)	(± 62.2)	(± 59.6)	(± 72.2)	(± 64.2)	(± 62.7)	(± 65.1)	(± 52.4)	(± 56.1)
Total Melt On Glaciers	113.9	118.7	133.4	128.0	122.5	94.8	57.4	34.1	11.6	0.0
	(± 21.3)	(± 10.9)	(± 18.2)	(± 13.7)	(± 16.7)	(± 15.7)	(± 11.4)	(± 7.4)	(± 9.5)	(± 0.0)
Glacier Melt	55.3	61.9	72.9	73.8	80.6	64.2	40.9	24.6	8.9	0.0
	(± 23.3)	(± 11.2)	(± 22.8)	(± 21.3)	(± 21.1)	(± 12.6)	(± 10.5)	(± 5.8)	(± 7.2)	(± 0.0)
Snow Melt On Glaciers	58.6	56.8	60.6	54.2	41.9	30.6	16.5	9.6	2.8	0.0
	(± 4.6)	(± 4.5)	(± 7.2)	(± 9.6)	(± 7.6)	(± 6.0)	(± 4.5)	(± 2.7)	(± 2.4)	(± 0.0)

https://doi.org/10.5194/egusphere-2025-3462
Preprint. Discussion started: 17 November 2025

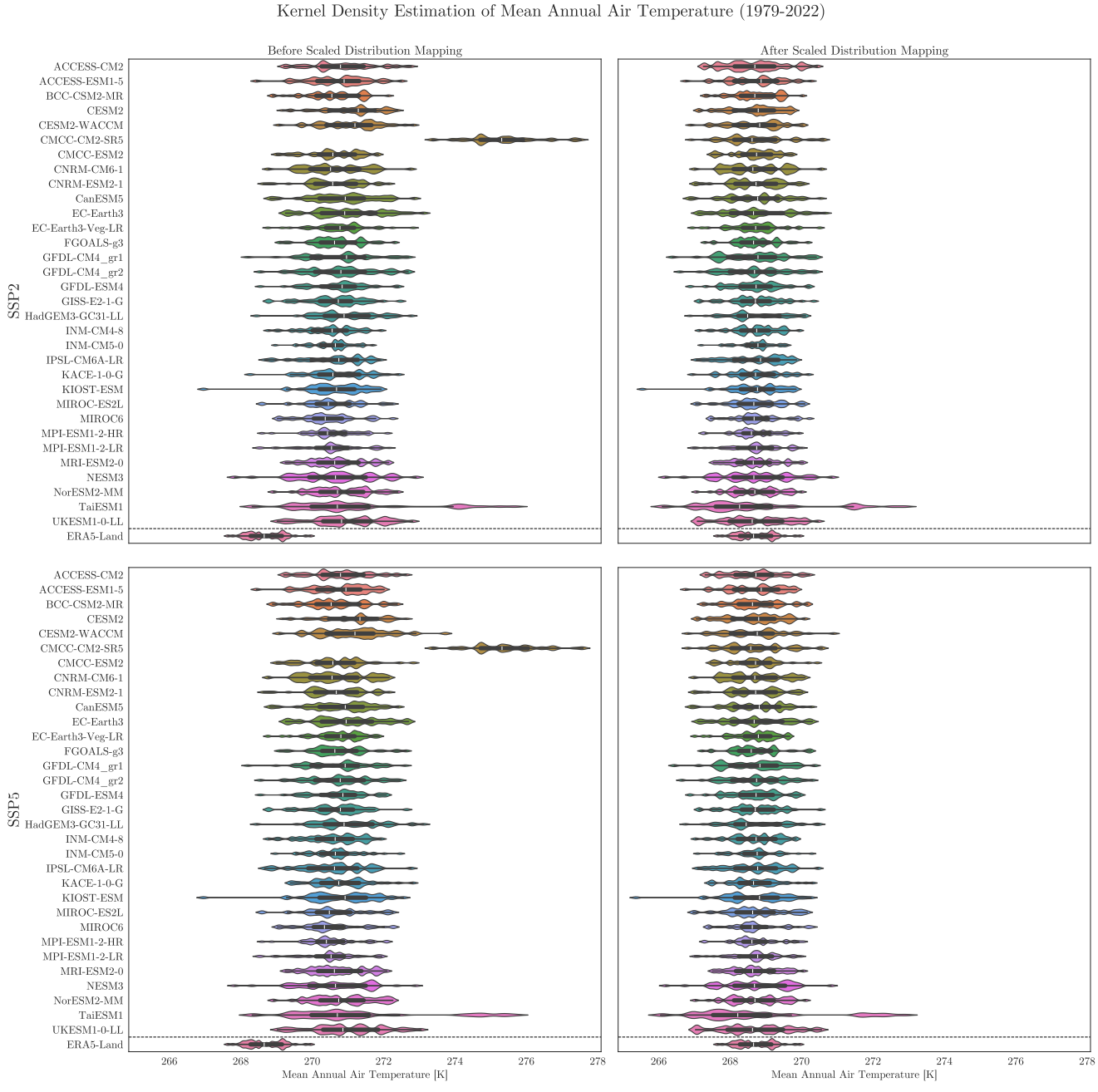

Figure A1. Kernel density estimation (KDE) for annual mean temperature of all CMIP6 ensemble members and ERA5-Land from 1979–2022 before and after bias adjustment.

https://doi.org/10.5194/egusphere-2025-3462
Preprint. Discussion started: 17 November 2025

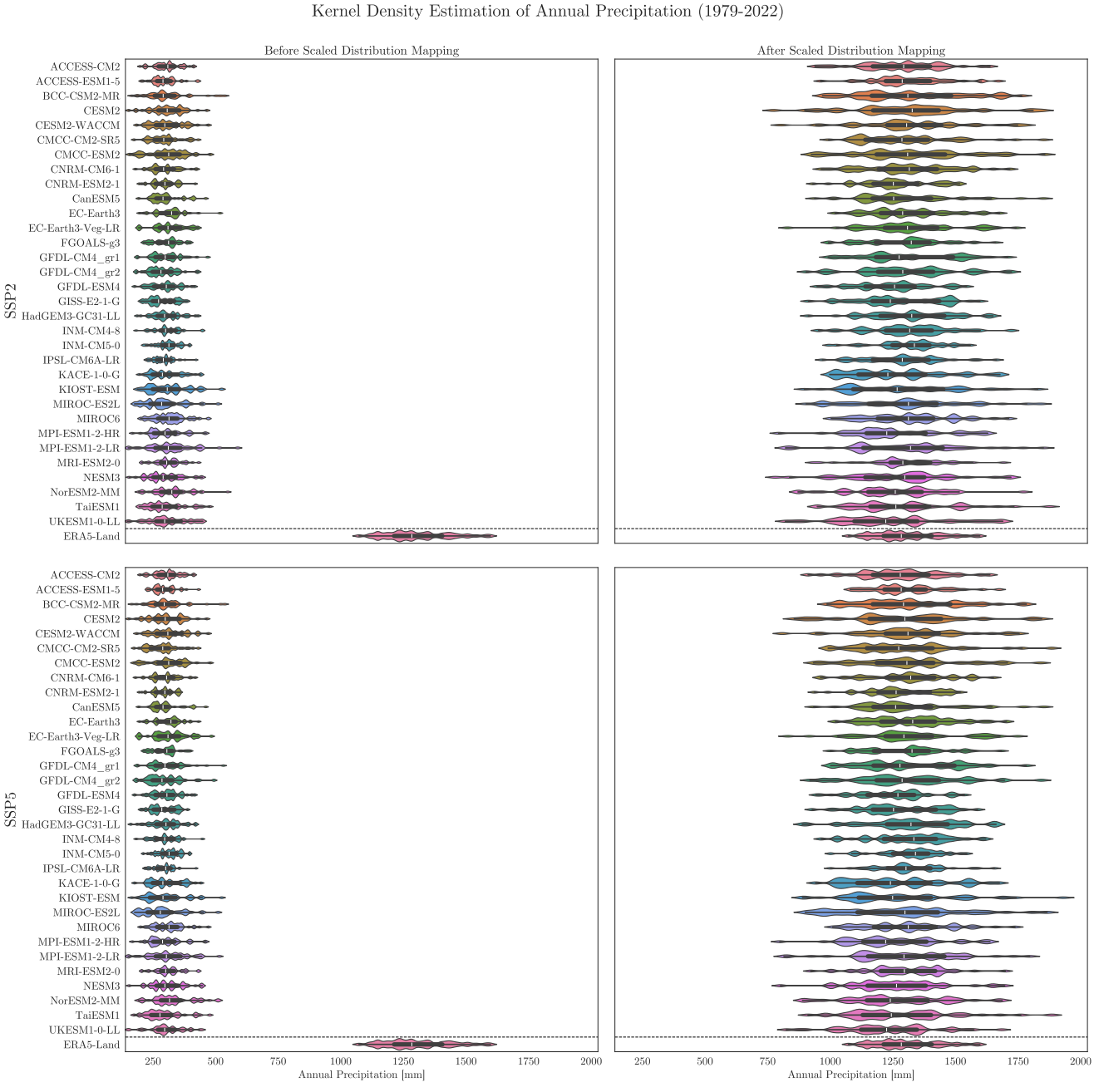

Figure A2. Kernel density estimation (KDE) for annual precipitation of all CMIP6 ensemble members and ERA5-Land from 1979–2022 before and after bias adjustment.

https://doi.org/10.5194/egusphere-2025-3462
Preprint. Discussion started: 17 November 2025

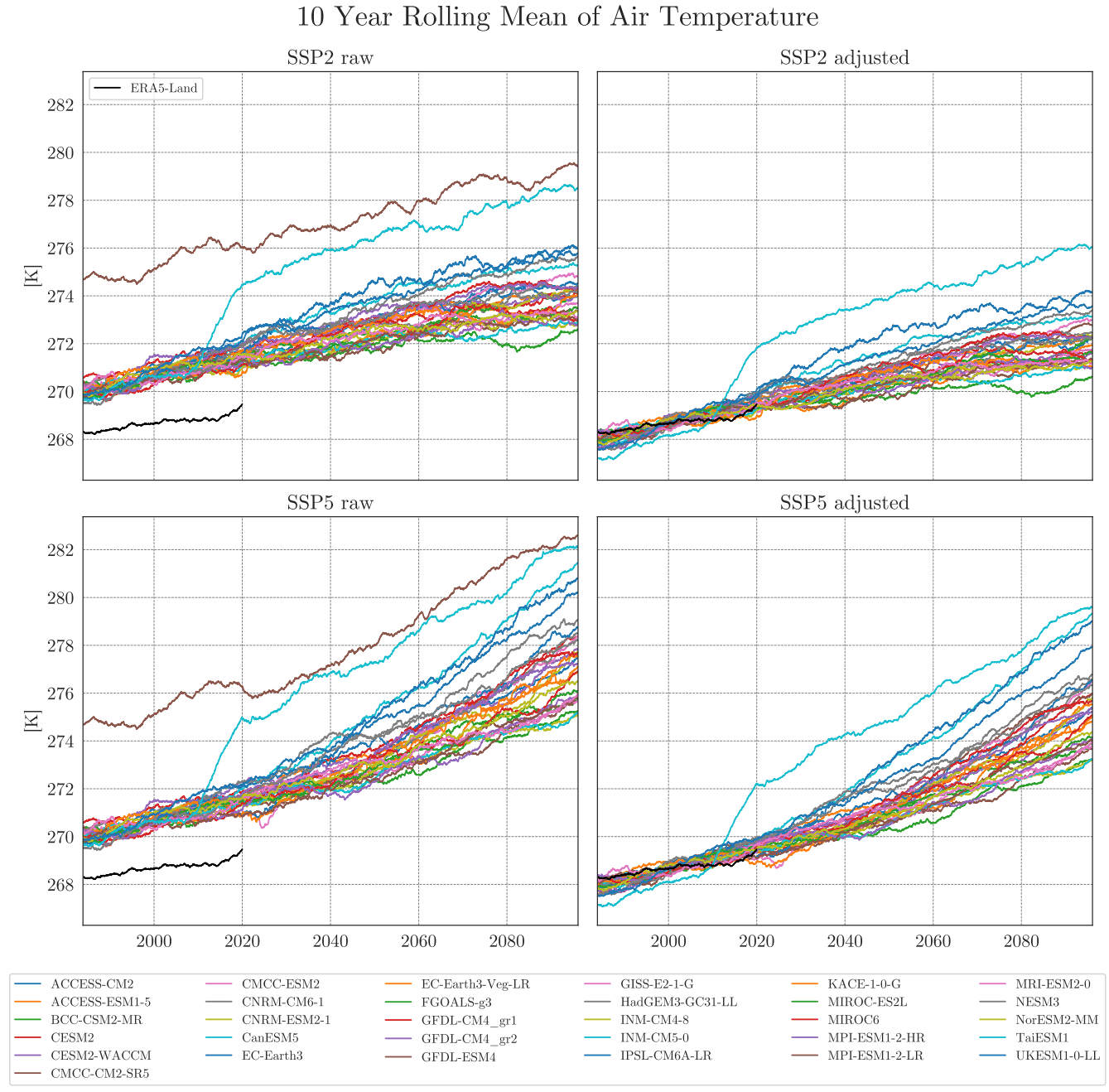

Figure A3. Ten year mean of air temperature of all CMIP6 ensemble members and ERA5-Land from 1979–2022 before and after bias adjustment.

https://doi.org/10.5194/egusphere-2025-3462
Preprint. Discussion started: 17 November 2025

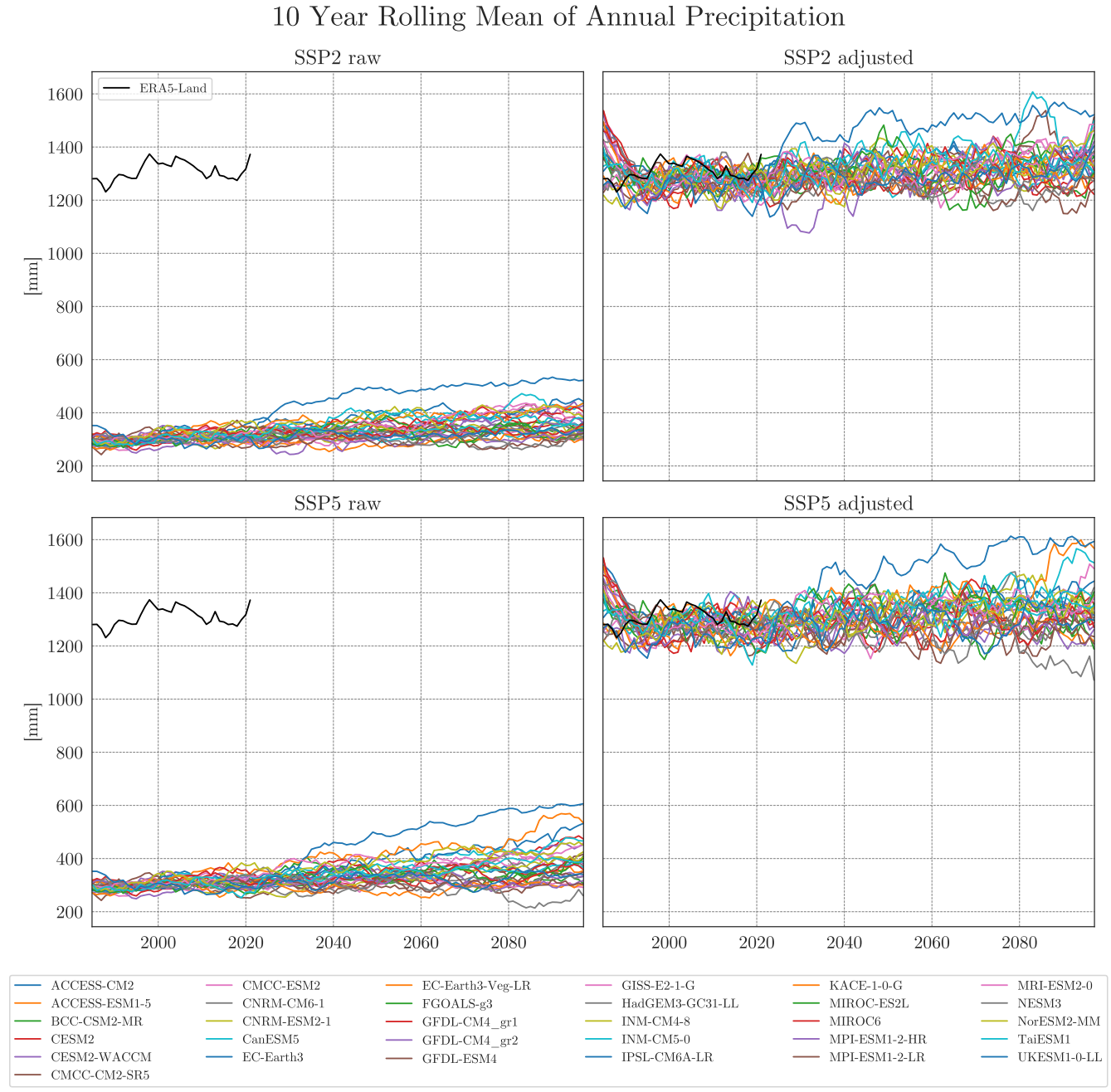

Figure A4. Ten year mean of monthly precipitation of all CMIP6 ensemble members and ERA5-Land from 1979–2022 before and after bias adjustment.

https://doi.org/10.5194/egusphere-2025-3462
Preprint. Discussion started: 17 November 2025

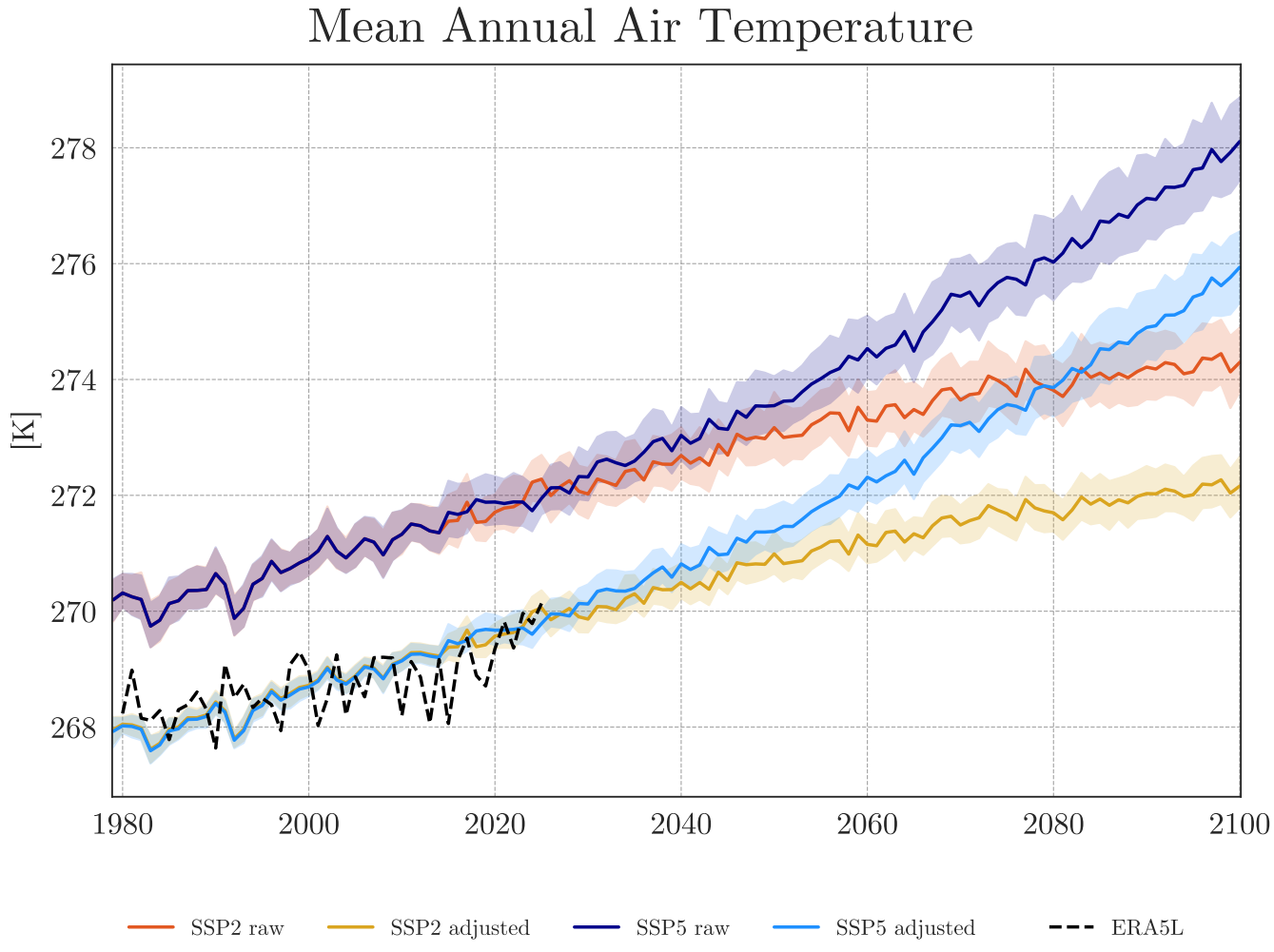

Figure A5. Mean annual air temperature of all CMIP6 ensemble members with 90% confidence interval and ERA5-Land from 1979–2022 before and after bias adjustment.

https://doi.org/10.5194/egusphere-2025-3462
Preprint. Discussion started: 17 November 2025

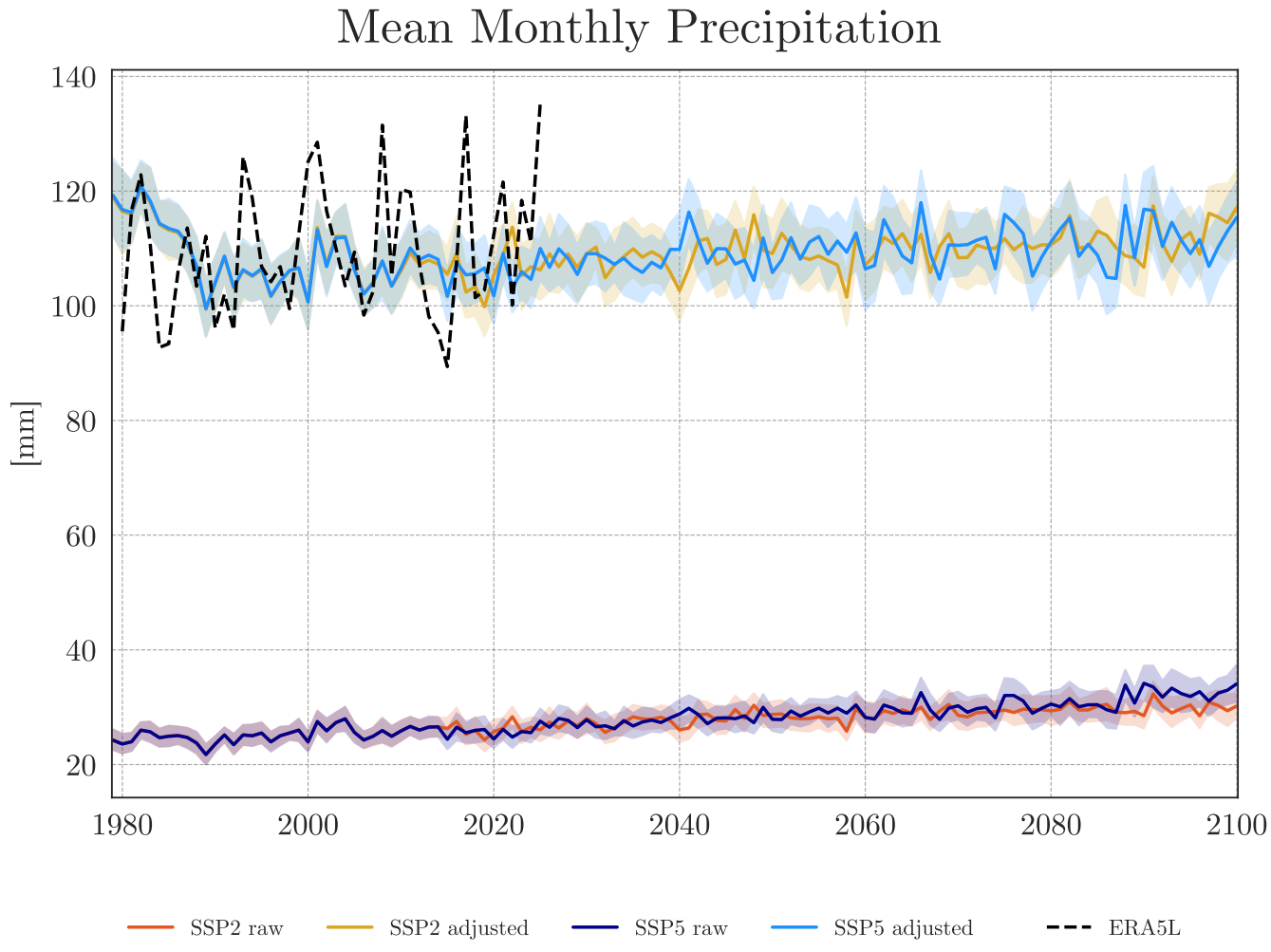

Figure A6. Annual mean of monthly precipitation of all CMIP6 ensemble members with 90% confidence interval and ERA5-Land from 1979–2022 before and after bias adjustment.

https://doi.org/10.5194/egusphere-2025-3462
Preprint. Discussion started: 17 November 2025

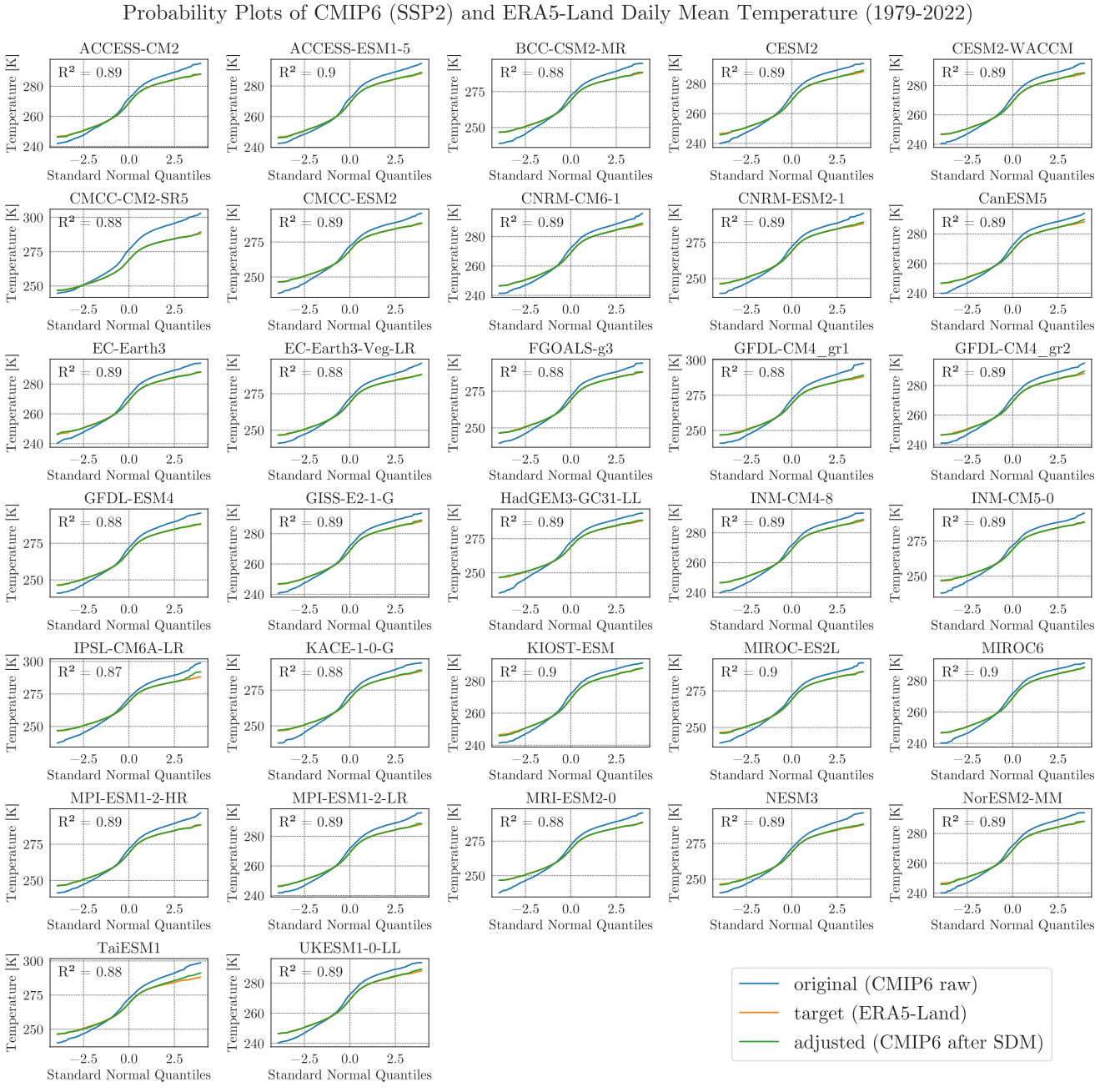

Figure A7. Probability plots of daily mean temperature under SSP2 for all CMIP6 ensemble members. The plots compare raw model data, reanalysis data, and bias-adjusted model data using standard normal quantiles. Pearson correlation coefficients (R^2) are shown for the latter two.

https://doi.org/10.5194/egusphere-2025-3462
Preprint. Discussion started: 17 November 2025

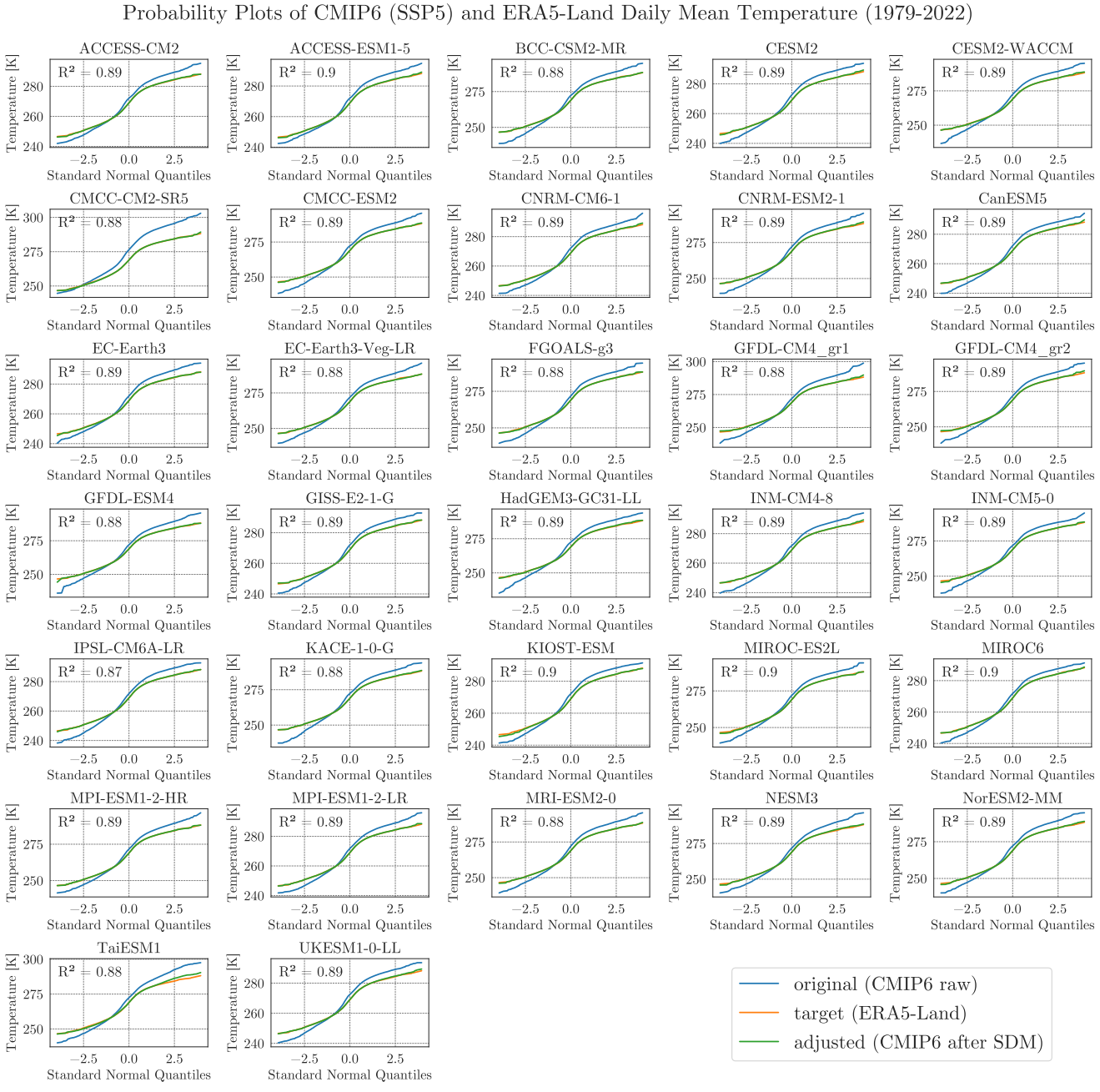

Figure A8. Probability plots of daily mean temperature under SSP5 for all CMIP6 ensemble members. The plots compare raw model data, reanalysis data, and bias-adjusted model data using standard normal quantiles. Pearson correlation coefficients (R^2) are shown for the latter two.

https://doi.org/10.5194/egusphere-2025-3462
Preprint. Discussion started: 17 November 2025

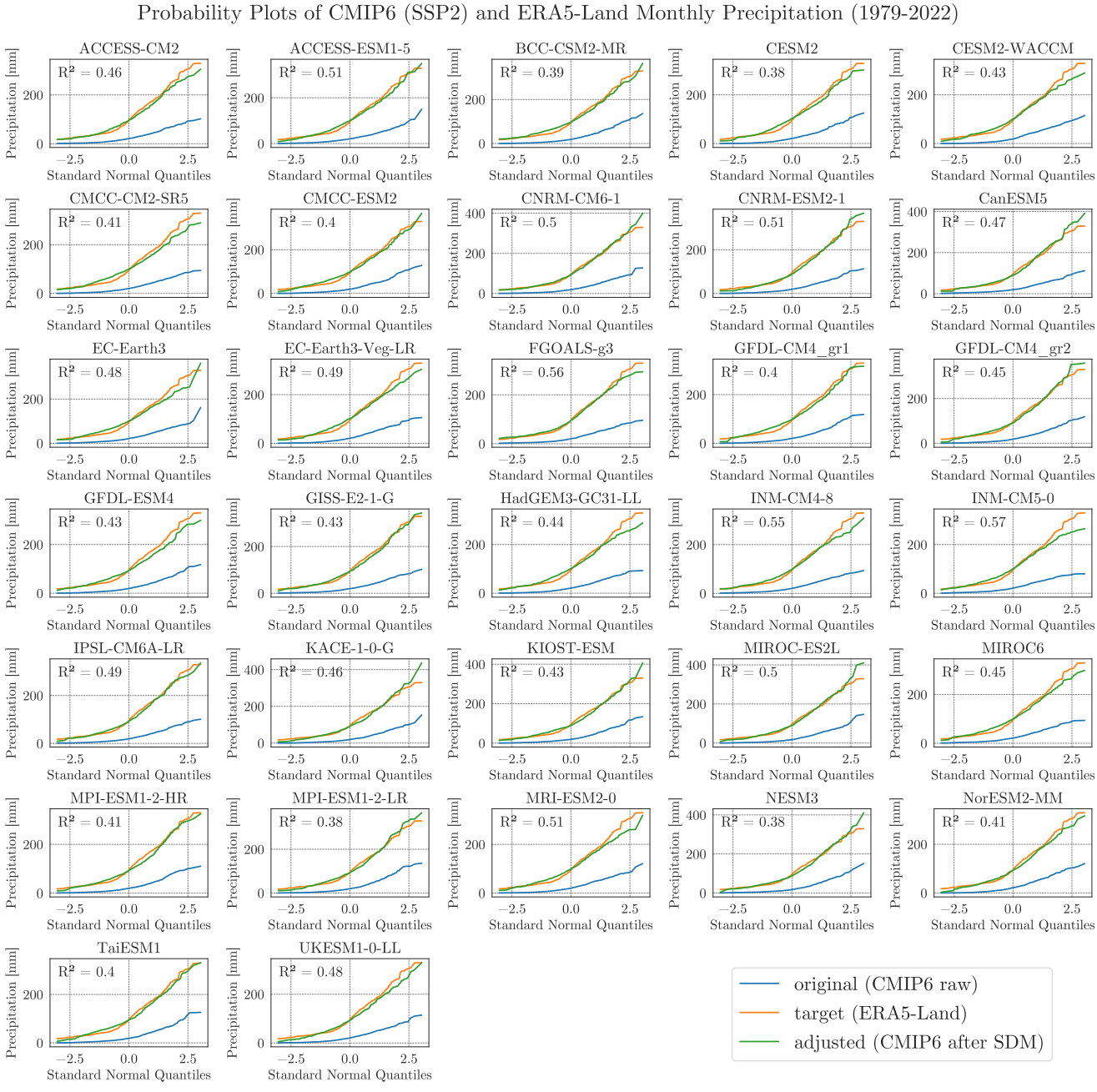

Figure A9. Probability plots of monthly precipitation under SSP2 for all CMIP6 ensemble members. The plots compare raw model data, reanalysis data, and bias-adjusted model data using standard normal quantiles. Pearson correlation coefficients (R^2) are shown for the latter two.

https://doi.org/10.5194/egusphere-2025-3462
Preprint. Discussion started: 17 November 2025

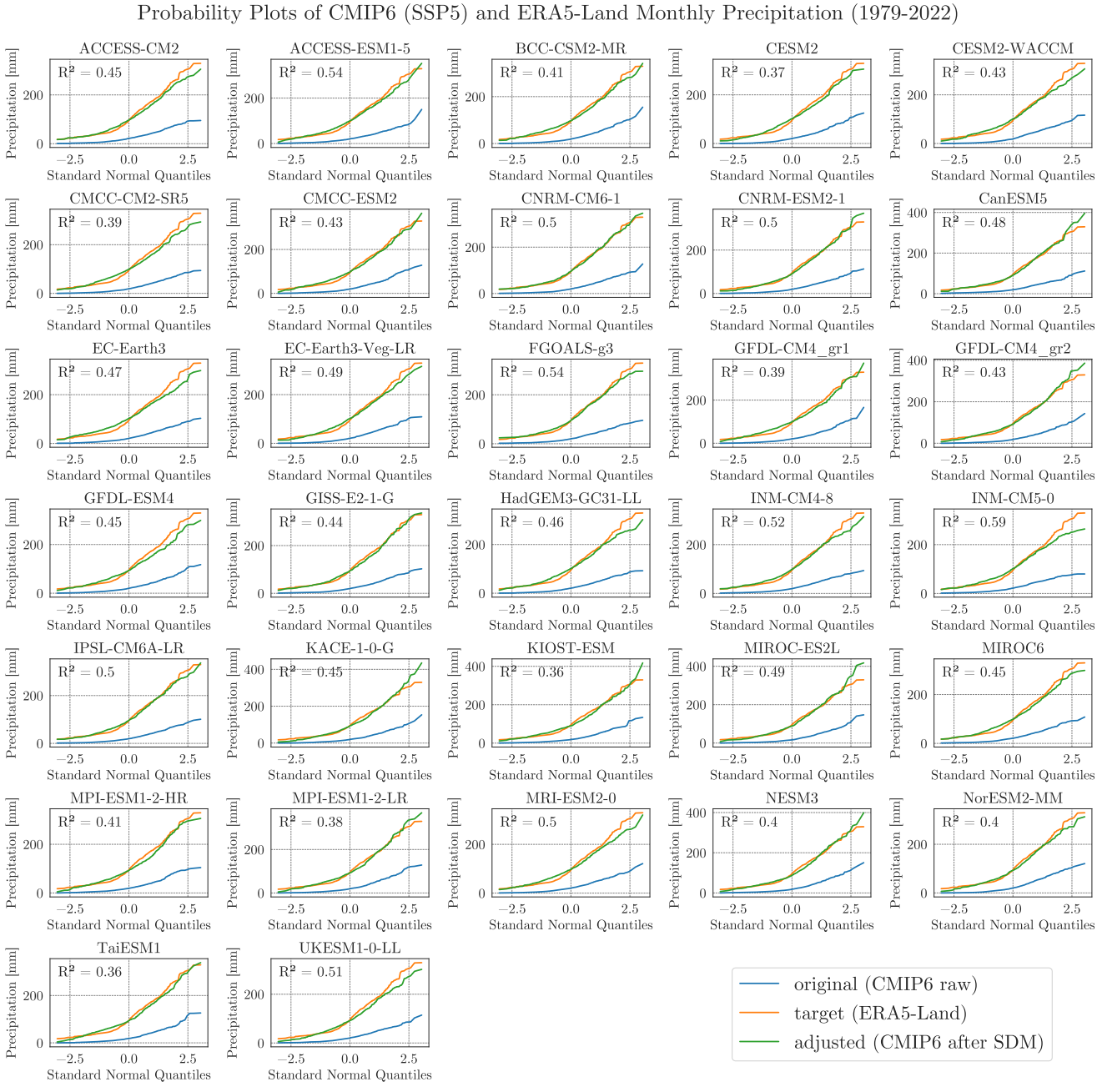

Figure A10. Probability plots of monthly precipitation under SSP5 for all CMIP6 ensemble members. The plots compare raw model data, reanalysis data, and bias-adjusted model data using standard normal quantiles. Pearson correlation coefficients (R^2) are shown for the latter two.

https://doi.org/10.5194/egusphere-2025-3462
Preprint. Discussion started: 17 November 2025

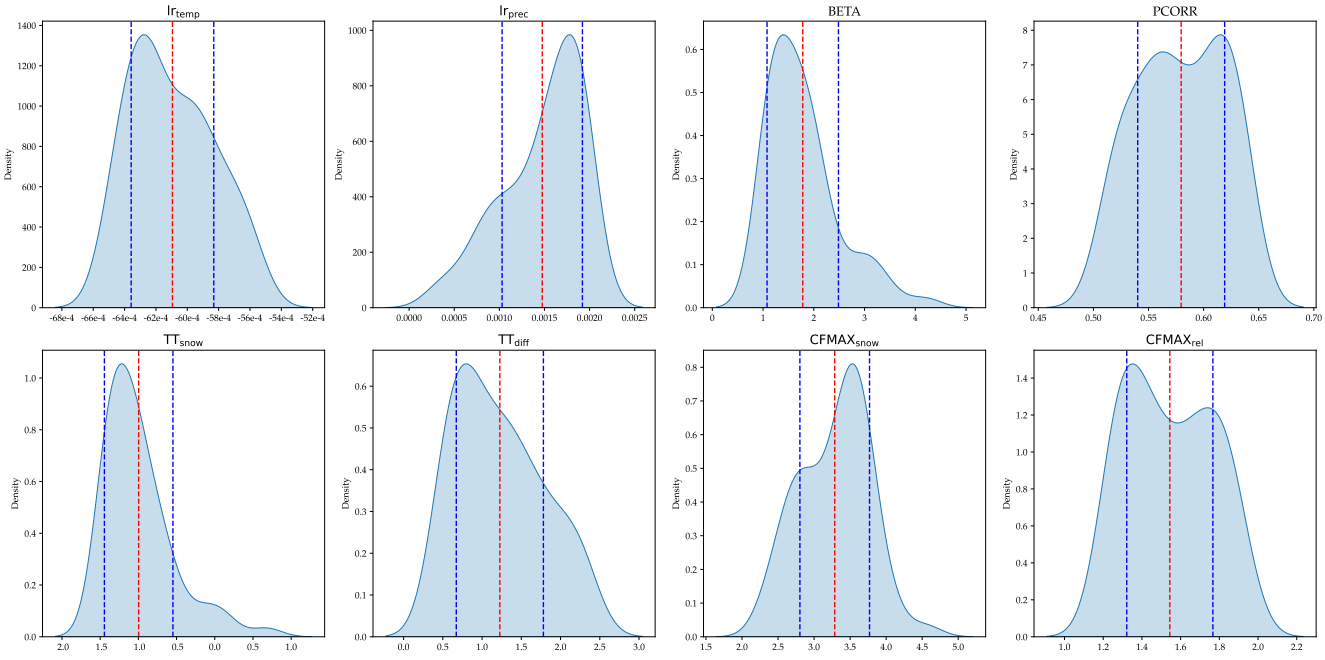

Figure A11. Posterior kernel density estimations (KDEs) of calibration step 1. Red dashed lines show the mean value of the posterior distribution. Blue dashed lines show the standard deviation from the mean in both directions.

https://doi.org/10.5194/egusphere-2025-3462
Preprint. Discussion started: 17 November 2025

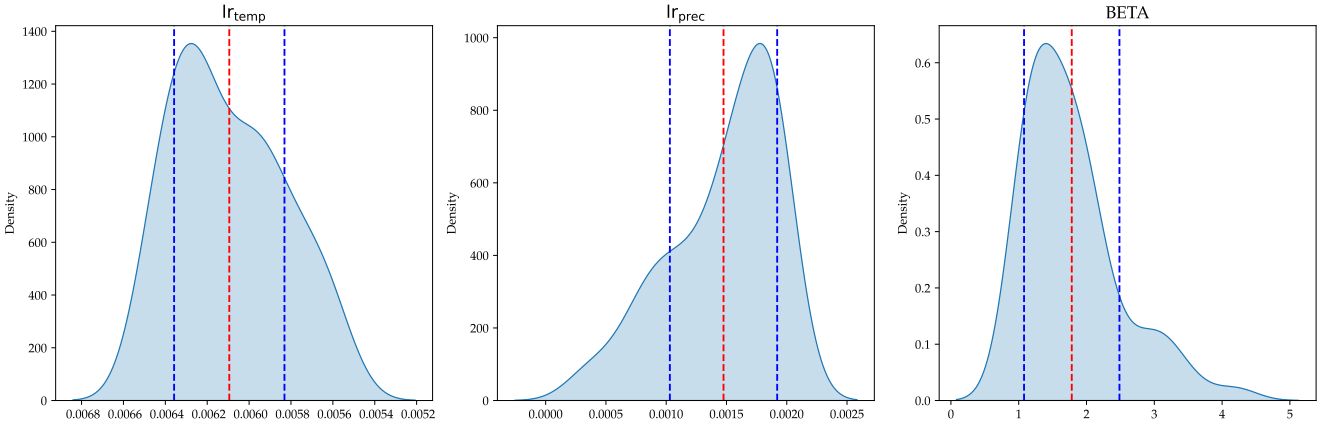

Figure A12. Posterior kernel density estimations (KDEs) of calibration step 2. Red dashed lines show the mean value of the posterior distribution. Blue dashed lines show the standard deviation from the mean in both directions.

https://doi.org/10.5194/egusphere-2025-3462
Preprint. Discussion started: 17 November 2025

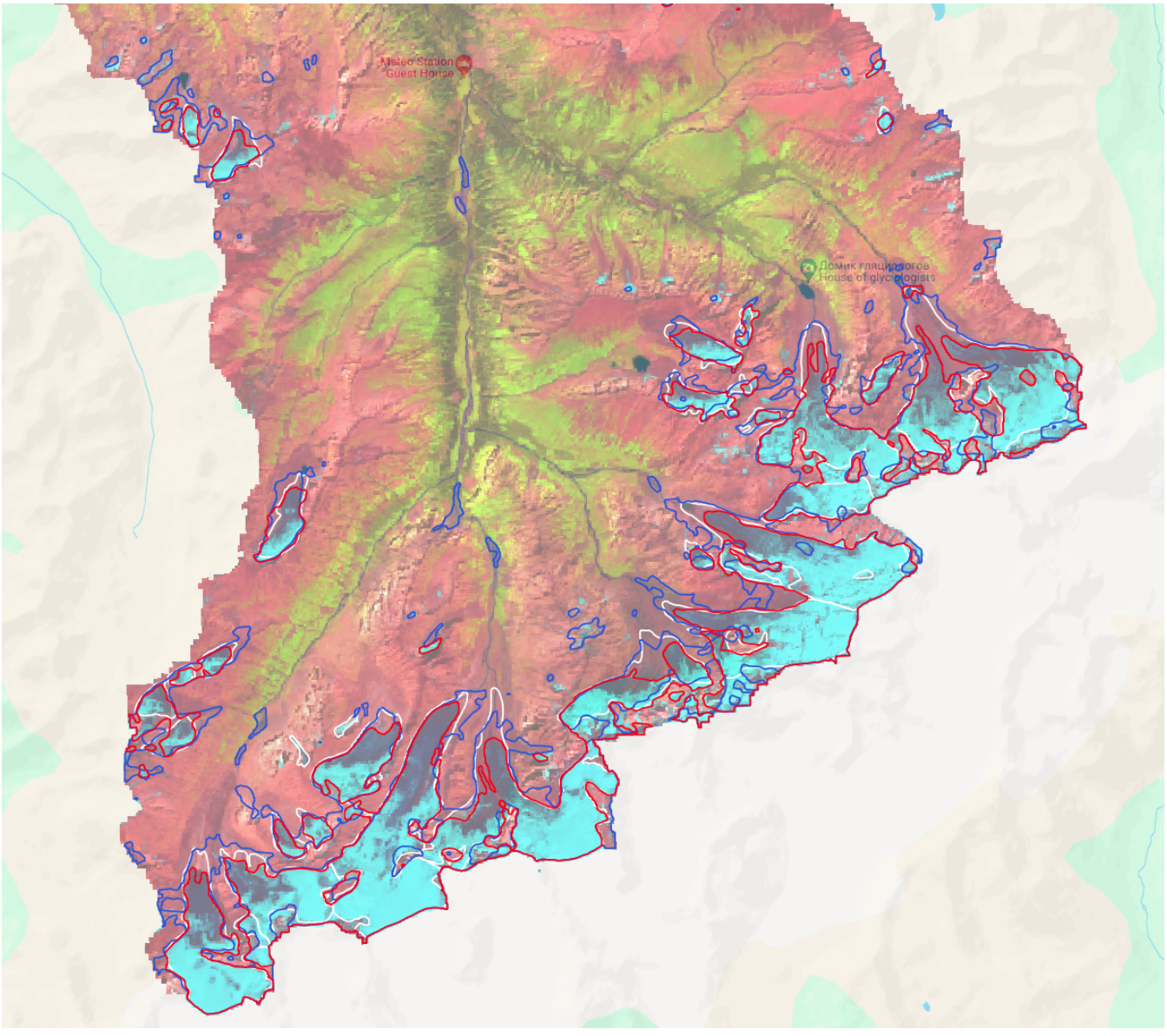

Figure A13. Results of the semi-automated random forest glacier mapping in the upper Kyzylsuu catchment. Glacier outlines based on a Landsat 7 image from August 25, 2002 shown in blue. Glacier outlines based on a Sentinel 2 image from July 21, 2022 shown in red. Glacier outlines according to the Randolph Glacier Inventory v6 referring to 2002 shown in white. The background false color image shows a band combination of the Sentinel-2 scene suitable to distinguish bare ice (dark blue) from snow (light blue). Base layer by Google ©2024.